Production of diverse brGDGTs by Acidobacterium *Solibacter usitatus* in response to temperature, pH, and O_2 provides a culturing perspective on brGDGT paleoproxies and biosynthesis

Toby A. Halamka[1]*, Jonathan H. Raberg[1], Jamie M. McFarlin[1], Adam D. Younkin[1], Christopher Mulligan[1], Xiao-Lei Liu[2], Sebastian H. Kopf[1]

[1]University of Colorado Boulder, Department of Geological Sciences
[2]University of Oklahoma School of Geosciences
*Corresponding Author: Toby A. Halamka (Toby.Halamka@colorado.edu)

Disclaimer: This manuscript is a non-peer reviewed preprint submitted to EarthArXiv. The authors have submitted this manuscript to Geobiology for consideration for publication. Following any peer-reviewed publication of this manuscript, the authors will provide a DOI to the publication.

Author Contributions: TAH, ADY and SHK designed the research. TAH, JMM, ADY, CM and SHK performed the research. XLL, TAH, JHR and SHK analyzed the data. TAH, JHR, XLL, and SHK wrote the paper.

Competing Interest Statement: The authors declare no competing interests.

Keywords: brGDGTs, Acidobacteria, Paleoclimate

This PDF file includes:

- Main Text including Figures 1 to 4
- Supplementary Figures S1 to S10
- Supplementary Tables S1 to S6

Abstract

Branched Glycerol Dialkyl Glycerol Tetraethers (brGDGTs) are bacterial membrane lipids that are frequently employed as paleoenvironmental proxies because of the strong empirical correlations between their relative abundances and environmental temperature and pH. Despite the ubiquity of brGDGTs in modern and paleo environments, the source organisms of these enigmatic compounds have remained elusive, requiring paleoenvironmental applications to rely solely on observed environmental correlations. Previous laboratory and environmental studies have suggested that the globally abundant bacterial phylum of the Acidobacteria may be an important brGDGT producer in nature. Here, we report on experiments with a cultured Acidobacterium, *Candidatus Solibacter usitatus*, that makes a large portion of its cellular membrane (~24% on average across experiments) out of a structurally diverse set of brGDGTs. *S. usitatus* was grown across a range of temperatures from 15 to 30°C, pH from 5.0 to 6.5 and O_2 from 1% to 21% and demonstrated pronounced shifts in the degree of brGDGT methylation. The observed temperature response in culture was in close agreement with trends observed in environmental samples, suggesting a physiological basis for the empirical connection between brGDGT methylation number and temperature. In contrast, culture pH had little effect on brGDGT cyclization, potentially indicating that changes in bacterial community composition underlie the link between cyclization number and pH observed in environmental samples. Varying oxygen concentrations altered brGDGT methylation number independent of temperature and resulted in the production of uncommon isomers, highlighting both the potential for this environmental parameter to skew paleotemperature reconstruction as well as the possible existence of brGDGT-based indicators of low O_2. Finally, genomic evidence and the production of brGTGTs (trialkyl tetraethers) in addition to previously discovered iso-C15 based mono- and di-ethers in *S. usitatus* suggest a new biosynthetic pathway for brGDGTs.

Introduction

Branched Glycerol Dialkyl Glycerol Tetraethers (brGDGTs) are a group of membrane-spanning non-isoprenoidal lipid biomarkers first characterized from peat (Sinninghe Damsté et al., 2000) and since discovered in virtually all modern environments including soils, lakes, rivers, hydrothermal settings, marine environments, and sedimentary systems (Lincoln et al., 2013; Weijers et al., 2006; Hopmans et al., 2004; De Jonge et al., 2014b; Tierney and Russell, 2009; Raberg et al., 2022a). Today, several structural variations of brGDGTs that differ in the number of cyclopentyl moieties, the number of methyl branches, and the position of some of the branches are routinely quantified in environmental samples and frequently used for paleoenvironmental reconstruction (e.g., Laurentano et al., 2021; Lu et al., 2019; Lindberg et al., 2021; Weijers et al., 2007; Peterse et al., 2012; Naafs et al., 2017b)

In environmental brGDGTs, the number of alkyl-chain methylations correlates strongly with temperature in numerous sample types, including soils (e.g., Naafs et al., 2017a), peats (e.g., Naafs et al., 2017b), lake sediments (e.g., Martínez-Sosa et al., 2021; Raberg et al., 2021) and marine sediments (Xiao et al., 2022). These changes in the number of methylations is commonly quantified by calculating indices such as the Methylation index of Branched Tetraethers (MBT) (Weijers et al., 2007; and MBT'_{5Me} De Jonge et al., 2014a) or by grouping brGDGTs into the structurally based Methylation (Meth) Set (Fig. S2; Raberg et al., 2021) for comparisons with environmental temperatures. A similar correlation has been observed between pH and cyclopentane ring number, as demonstrated by the Cyclization index of Branched Tetraethers (CBT) and related indices (e.g., CBT_{5Me}; De Jonge et al., 2014a) or the Cyclization (Cyc) Set (Fig. S2; Raberg et al., 2021). Additionally, conductivity/salinity has been shown to correlate with the positions of alkyl-chain methylations (Raberg et al., 2021; Wang et al., 2021). Finally, other environmental parameters, most notably dissolved oxygen (Weber et al., 2018; Wu et al., 2021; Liu et al., 2014; Martínez-Sosa and Tierney 2019), can influence brGDGT distributions in nature, adding complexity to the

observed relationships with temperature/pH and posing both new challenges and new opportunities for proxy applications.

Despite more than 20 years of work on environmental brGDGTs, the source organisms of these ubiquitous compounds remain largely unknown. Though brGDGTs are structurally similar to membrane-spanning isoprenoidal glycerol tetraethers produced by Archaea, the stereochemistry of the glycerol backbone of brGDGTs points to a bacterial source (Weijers et al., 2006). Amongst the myriad bacterial heterotrophs that exist in nature, the phylum Acidobacteria has gained the most attention as a potential source group, however, other phyla of soil bacteria often with equally poor representation in culture collections cannot be dismissed as potential brGDGT-producers. Environmentally observed brGDGT patterns could be the result of microbial community shifts, the physiological responses of a specific taxonomic group, or a combination of both (De Jonge et al., 2019; De Jonge et al., 2021; Guo et al., 2022).

In soil environments, Acidobacteria frequently represent more than 20% of all classified bacterial sequences and as high as 70% in some acidic environments (Jones et al., 2009) with community sequencing in environmental samples and laboratory mesocosms showing strong correlations in Acidobacteria populations with the production of brGDGTs (Weijers et al., 2010, Martínez-Sosa and Tierney, 2019; Weber et al., 2018; De Jonge et al., 2021). Unfortunately, the isolation and subsequent laboratory cultivation of Acidobacteria has proven difficult, resulting in only a small pool of cultured representatives (George et al., 2011) with still no pure cultures available for more than half of the 26 major taxonomic subdivisions (SDs; Barns et al., 2007). Insights about the physiology and likely heterotrophic and mostly aerobic lifestyle of the Acidobacteria is thus largely built on genomic analyses (Eichorst et al., 2018) and culturing work with a relatively small group of SD 1, 3, 4, 6 and 8 pure cultures. Laboratory studies with the available strains revealed several likely brGDGT precursor lipids found within the phylum (Sinninghe Damsté et al., 2011) including abundant ether-bound lipids in SD 4 cultures (Sinninghe Damsté et al., 2014; Sinninghe Damsté et al., 2018) and the identification of at least one common

brGDGT (brGDGT Ia) in two SD 1 strains (Sinninghe Damsté et al., 2011) that is produced in response to low O2 in one of them (Halamka et al., 2021).

Despite these discoveries and ongoing efforts to isolate new Acidobacteria and other soil microorganisms, no organism that produces the wide range of brGDGT structures found in nature and used in paleoproxies has emerged. The lack of a biological model system to study brGDGT production and biological function in controlled laboratory experiments prevents probing of brGDGT-based proxies and limits their robustness and potential breadth of application.

As part of our research into the effects of low O_2 on brGDGT production (Halamka et al., 2021), we investigated several cultured Acidobacteria that harbor low affinity terminal oxidases in their genomes including the SD3 Acidobacterium *Candidatus Solibacter usitatus* (Joseph et al., 2003), hypothesizing that they might be adapted to low O_2 environments. Here we report the production of the common brGDGTs Ia, IIa, IIIa, Ib, and IIb as well as several uncommon tetraethers in *S. usitatus*. The branched tetraethers comprise a significant fraction of the organism's cellular membrane (24 ± 9% on average across all experimental conditions) and change in relative abundance in response to physiological constraints including temperature, pH, and O_2, allowing a direct comparison with brGDGT-based paleo-proxies. We demonstrate that the degree of brGDGT methylation in *S. usitatus* in response to temperature variations is in agreement with empirically-developed environmental proxies. However, we find that the degree of brGDGT cyclization in *S. usitatus* in response to pH does not match environmental trends. Finally, we show that *S. usitatus* makes several brGDGT structures that correlate to changes in O_2.

Materials and Methods

Microbial Strains, Media, and Growth Conditions

Candidatus Solibacter usitatus strain Ellin6076 (Joseph et al. 2003) was acquired from the German Collection of Microorganisms and Cell Cultures (DSM 22595) and was grown in triplicate in a modified DSMZ 1266 medium at all temperature, pH, and oxygen conditions. Modified DSMZ 1266 medium consisted of 13. 3mM MES buffer, 0.67g/L Yeast Extract (YE), 2.5 mM Glucose, 0.27 mM $MgSO_4$, 0.4 mM $CaCl_2$, 0.2 mM KH_2PO_4, 0.4 mM NH_4Cl, 15 nM (3 µg/L) Na_2SeO_3, 16 nM (4 µg/L)

103 Na_2WO_4, 1.33 mL/L SL10 trace element solution, and 1.33 mL/L HS Vitamin solution. SL10 trace
104 element solution: 1.5 g/L $FeCl_2$ x 4 H_2O, 70 mg/L $ZnCl_2$, 100 mg/L $MnCl_2$ x 4 H_2O, 6 mg/L H_3BO_3,
105 190 mg/L $CoCl_2$ x 6 H_2O, 2 mg/L $CuCl_2$ x 2 H_2O, 24 mg/L $NiCl_2$ x 6 H_2O, 36 mg/L Na_2MoO_4 x 2
106 H_2O. HS Vitamin solution: 50 mg/L alpha-Lipoic acid (thioctic acid), 50 mg/L Biotin / D+ biotin, 100
107 mg/L Ca-pantothenate (D+), 50mg/L Cyanocobalamin (B12), 50 mg/L Folic acid, 100 mg/L Nicotinic
108 acid (Niacin), 100 mg/L p/4-Aminobenzoic acid, 100 mg/L Pyridoxine Hydrochloride, 100 mg/L
109 Riboflavin, 100 mg/L Thiamine Hydrochloride. Media pH was adjusted with 5M NaOH and cultures
110 were buffered using 2-(*N*-morpholino) ethanesulfonic acid (MES). Growth was monitored using
111 optical density (OD) measurements. Routine OD measurements were taken at 600 nm for aerobic
112 culture tubes and 630 nm in 100 mL bottles. Growth rates were calculated for all replicate cultures
113 by fitting OD measurements to the logistic equation (Table S2). Suboxic headspace in 100 mL
114 bottles was achieved by continuously flushing the culture headspace at a rate of 100mL/min with
115 high purity N_2 blended with compressed air using digital mass flow controllers. The gas blend for ~
116 1% O_2 cultures consisted of 95% N_2 and 5% air (v/v), and the gas blend for ~5% O_2 cultures
117 consisted of 75% N_2 and 25% air (v/v). The long duration of these growth experiments required
118 that gas was bubbled through sterile water prior to entering the culture vessels to prevent rapid
119 evaporation of culture media.

120 **Lipid Extraction and Analysis**

121 Harvested cells were extracted using the rapid acidic hydrolysis-methanolysis protocol described
122 in Halamka et al. (2021). Cells from liquid culture were harvested in stationary phase by
123 centrifugation (5000 RPM for 3 minutes). Harvested cells were lyophilized overnight and then
124 physically disrupted in 2 mL microcentrifuge tubes by vortexing with methanol (MeOH) and 250 µL
125 of 100 µm muffled glass beads for 10 minutes at 3000 rpm using a Disruptor Genie (Scientific
126 Industries, SI-DD38). Excess MeOH was evaporated and 25 µg 23:0 PC (1,2-ditricosanoyl-sn-
127 glycero-3-phosphocholine), 25 µg 24:0 FA (tetracosanoic acid), and 25 ng C46 GTGT (Huguet et
128 al., 2006) were added to all samples as internal quantification standards. Lipids were extracted for
129 90 minutes at 65 °C with 500 µL 3N hydrochloric acid (HCl) in MeOH (33 % final water content) to

130 cleave tetraether headgroups and transesterify fatty acid esters to fatty acid methyl esters (FAMEs).
131 Samples were cooled for 10-minutes before the addition of 500 µL methyl tert butyl ether. The
132 upper organic phase was extracted 3 times with 500 µL n-hexane and total lipid extracts (TLEs)
133 were evaporated under N_2.

134 Mono-Acyl Glycerol Ethers (MAGEs, or mono-ethers) and Di-Acyl Glycerol Ethers (DAGEs,
135 or di-ethers) were acetylated for Gas Chromatography (GC) analysis by suspending in 100 µL of
136 Dichloromethane (DCM) with the addition of 20 µL anhydrous pyridine and 20 µL of acetic
137 anhydride. Samples were then incubated at 70 °C for 20 minutes before evaporation and
138 resuspension in n-hexane for analysis. FAMEs, MAGEs, and DAGEs were analyzed in the CU
139 Boulder Earth Systems Stable Isotope Lab on Thermo Trace 1310 GCs using an SSL injector and
140 a 30m DB-5 HT capillary column (Agilent Technologies, 0.25 mm I.D., 0.25 µm film thickness; 2
141 min at 40 °C, ramped to 295 °C at 15 °C/min, ramped to 315 °C at 5 °C/min, ramped to 375 °C at
142 15 °C/min then held for 5 min at 375 °C). Compounds were identified based on retention times of
143 authentic standards or by their mass spectra using a Thermo Scientific ISQ Single Quadrupole
144 Mass Spectrometer on full scan mode. All compounds were quantified by Flame Ionization Detector
145 (FID).

146 Tetraethers were analyzed in the Organic Geochemistry Laboratory at the University of
147 Colorado Boulder on a Thermo Scientific Ultimate 3000 High Performance Liquid Chromatograph
148 (HPLC) coupled to a Q Exactive Focus Orbitrap-Quadrupole MS with an Atmospheric Pressure
149 Chemical Ionization (APCI) source using a previously published normal phase (NP) methods
150 (Hopmans et al., 2016) with the following modification: the initial eluent gradient was 14 % 90:10
151 Hexane:IPA instead of 18 % 90:10 Hexane:IPA in order to achieve better separation between
152 isomers. The compounds were confirmed together with retention time and MS/MS spectra
153 generated by data dependent acquisition mode (ddMS/MS). A subset of the TLE samples was also
154 analyzed by reverse phase (RP) LC (Liu et al., 2019) to confirm relative elution order of brGDGT
155 isomers and further constrain their identity (data not shown). Cellular tetraether abundances were
156 calculated relative to fatty acids and mono/di-ethers using the C24 and C46 internal standards.

Environmental Samples and brGDGT Indices

BrGDGT distributions, temperature, and pH of environmental samples were selected from a compiled dataset (Raberg et al., 2022b). We selected the six most abundant sample types (soil, peat, lacustrine sediment, lacustrine settling/particulate matter, marine sediment, and bone) for comparison with *S. usitatus*. Temperature parameters for environmental samples were standardized where possible but are (necessarily) different for some sample types (e.g., sea surface temperature versus air temperature); all parameters were selected according to Raberg et al. (2022a). Soils with *in situ* temperature data were compiled from Wang et al. (2020), Pérez-Angel et al. (2020), De Jonge et al. (2019), Sigurdsson et al. (2016), Wang and Liu (2021), and Halfmann et al. (2022). The brGDGT indices MBT'_{5Me} (De Jonge et al., 2014a), CBT_{5Me} (De Jonge et al., 2014a), and degree of cyclization (DC; Baxter et al., 2019), were calculated as follows:

$$MBT'_{5Me} = (Ia + Ib + Ic) / (Ia + Ib + Ic + IIa + IIb + IIc + IIIa) \quad \text{(Eq. 1)}$$

$$CBT_{5Me} = - \log((Ib + IIb) / (Ia + IIa)) \quad \text{(Eq. 2)}$$

$$DC = (Ib + 2 * Ic + IIb + IIb') / (Ia + Ib + Ic + IIa + IIa' + IIb + IIb') \quad \text{(Eq. 3)}$$

BrGDGT fractional abundances in the Methylation and Cyclization Sets were calculated according to Raberg et al. (2021). Broadly, for brGDGT with roman numeral *x* (I, II, or III) and letter *y* (a, b, or c), the fractional abundance *f* in a given structural set *S* is calculated as,

$$fxy_S = xy / \text{sum(brGDGTs in S)} \quad \text{(Eq. 4)}$$

Structural Sets are defined in Figure S2.

Results

Occurrence of brGDGTs in *Solibacter usitatus*

S. usitatus grew successfully under all tested conditions except for pH 6.5 at 15°C. The organism's specific growth rate ranged from 0.23 day^{-1} at pH 6.0, 15°C and 21% O_2 to 1.45 day^{-1} at pH 5.5, 30°C and 21% O_2. Growth rates increased systematically from low to high growth temperatures and decreased systematically from high to low O_2 (Table S1, Fig. S1). *S. usitatus* produced a range of saturated, monounsaturated and terminally methyl-branched fatty acids as well as several mono- and di-ether but no iso-diabolic acid (13,16-dimethyl octacosanedioic acid) or its mono-glycerol-

bound equivalents (Table S3, Fig. S3), in agreement with the results of previous work on this organism (Sinninghe Damsté et al., 2018). In addition, we detected a wide range of tetraethers comprising an estimated 10% to 47% of the cellular membrane of *S. usitatus* across a range of temperature, pH, and oxygen conditions. Whereas brGDGTs were only detected under low oxygen growth conditions in *Edaphobacter aggregans* (Halamka et al., 2021), these lipids were abundant in *S. usitatus* at both low and high oxygen concentrations. Overall, tetraethers were most abundant at lower pH, lower temperature and lower O_2 (Table S2, Fig. S3).

Five of the 15 commonly studied brGDGTs – Ia, IIa, IIIa, Ib, and IIb – were abundant in *S. usitatus* cultures (Fig. 1a, Table S3). Mass traces of brGDGTs IIIb, Ic, IIc, and IIIc were also identified in the primary testing conditions, but at abundances nearing the detection limit and consequently irrelevant to paleoproxy testing. Though 6-methyl isomers of brGDGTIIa-c and IIIa-c are common in environmental samples (De Jonge et al., 2013), none were detected here, with all additional methylations at C5. However, *S. usitatus* produced several uncommon brGDGT isomers (Fig. 1a; see caption for isomer notation), with potential additional methylations at unconfirmed positions. While the abundance and condition-specific presence of these isomers likely influence the physiological properties of the cellular membrane of *S. usitatus*, we have omitted them from calculations relevant to current brGDGT paleoproxies as these equations focus on the 'primary' or 'conventional' brGDGT structures shown in Fig. 1c.

The identities of the above compounds were confirmed in *S. usitatus* by their corresponding retention times to brGDGTs of a reference soil extract, accurate masses, and fragmentation patterns in MS/MS. The brGDGT structural types, isomers, and NP-LC retention properties of *S. usitatus* and an in-house soil standard are shown in Fig. 1a. Growth rates for each fully oxygenated condition tested and the resultant structures of primary brGDGTs are shown in Fig. 1b and 1c, respectively (see Table S2 and Fig. S2 for further details on growth rates). This study subsequently focuses on the membrane compositional response of *S. usitatus* across a 15 °C temperature

gradient (15 °C - 30 °C), 1.5 unit pH gradient (pH 5.0 - 6.5), and dissolved oxygen gradient ranging from 1% O_2 to 21% O_2.

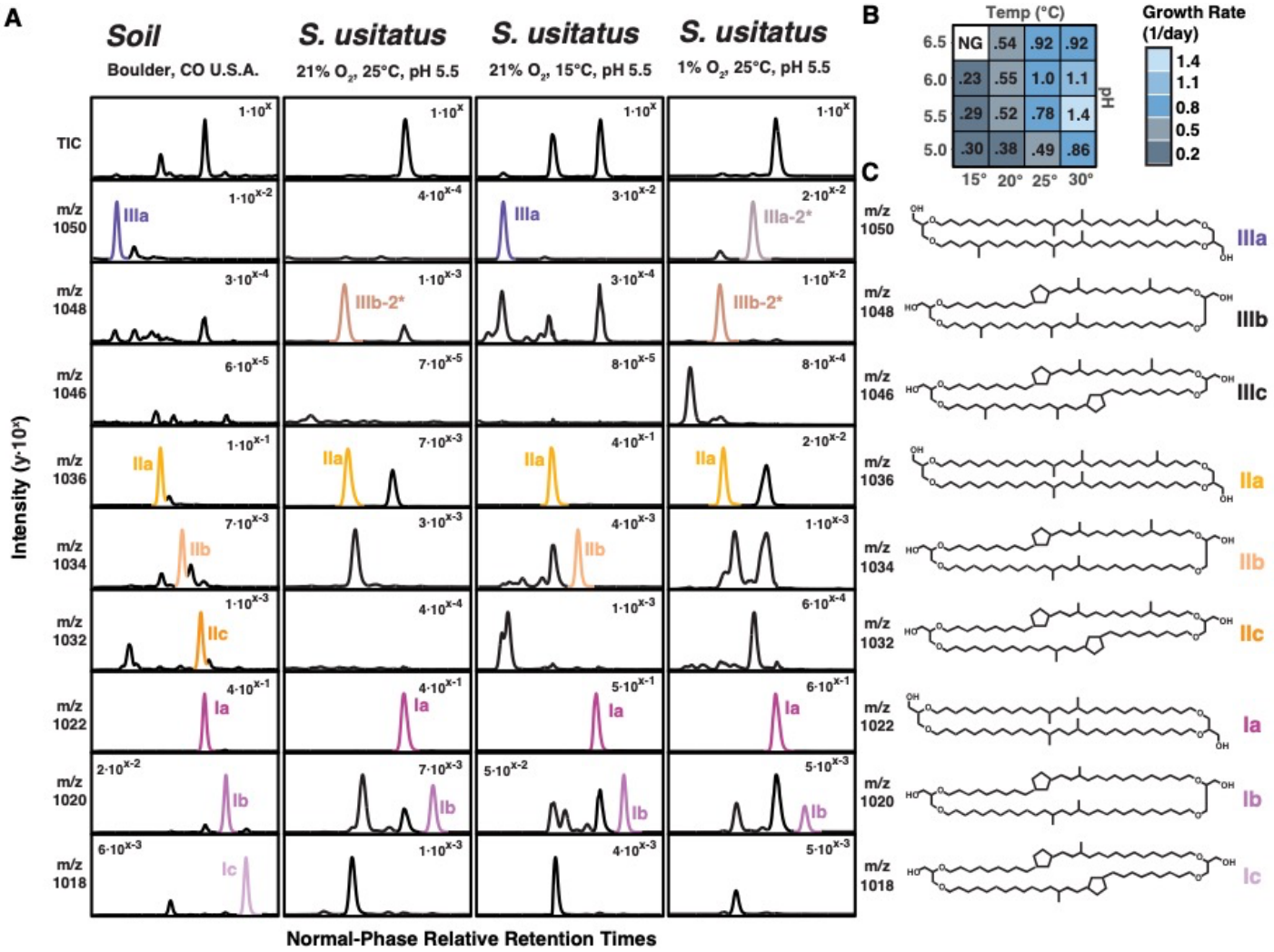

Figure 1. *Mass channel extracted chromatography, culturing growth rates, and brGDGT structures of S. usitatus and a soil reference standard. A) Selected mass channels of major brGDGT NP-HPLC-MS chromatographic retention times from a soil reference standard and three culturing conditions of S. usitatus. Selected brGDGT peaks are color-coded with corresponding color labels. Retention times reported as relative to brGDGTIa within each sample. Peak intensities reported as* $y{\cdot}10^x$ *for comparison between samples run at different concentrations. B) Overview of aerobic culturing conditions analyzed for this study with averaged growth rates (1/hr) of biological triplicates. C) Structures of major brGDGTs, with additional methylations at 5C. Compound label coloring consistent with peak and label coloring used in panel A. *notation describing brGDGT isomers that are structurally characterized in Fig. 3.*

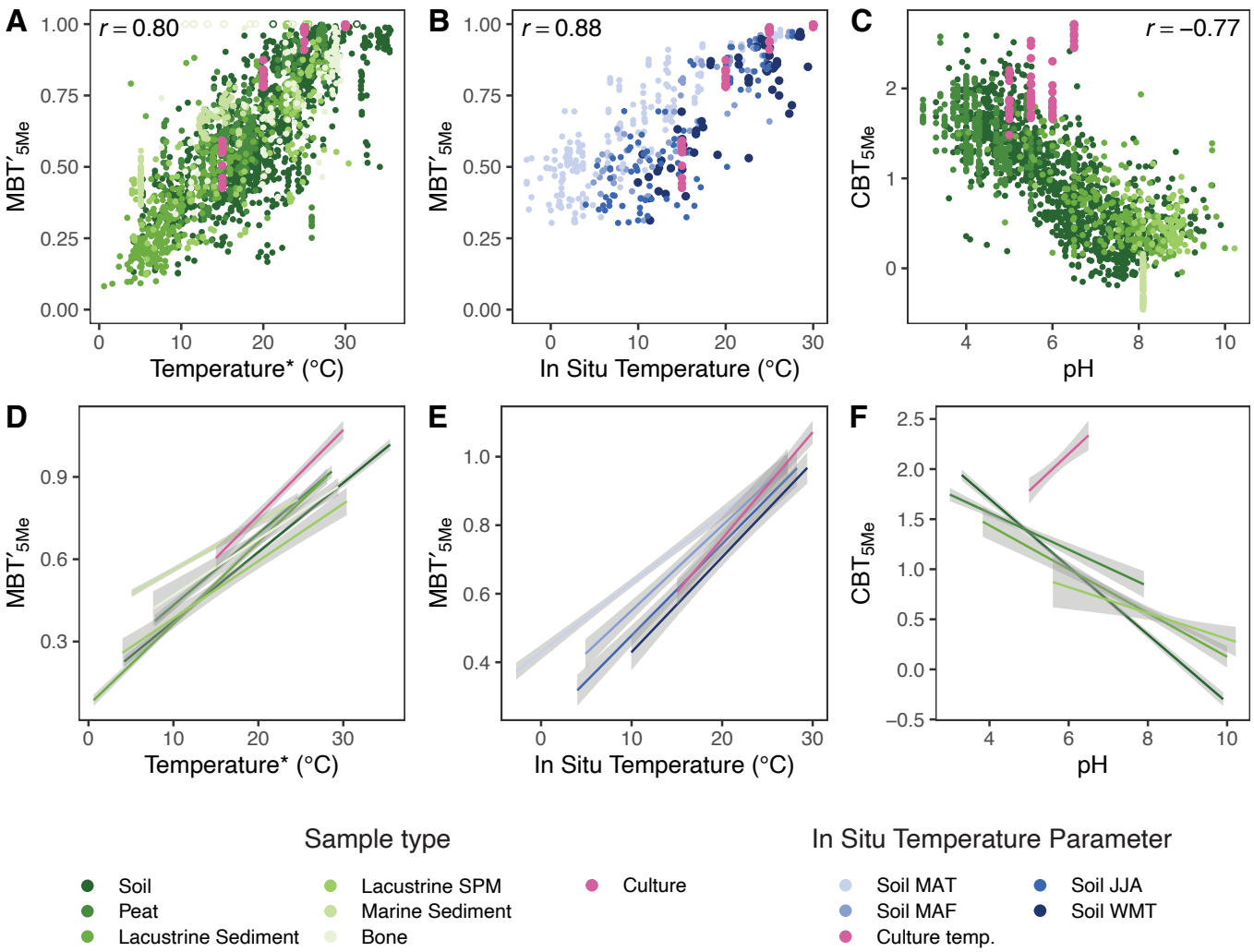

Figure 2. *Relationships between brGDGTs and temperature and pH for S. usitatus cultures and environmental samples. A) Relationship between the MBT'$_{5Me}$ index and temperature for cultures (pink) and environmental samples (green; SPM = suspended/settling particulate matter). *Temperatures were associated with environmental samples following Raberg et al. (2022a). Samples with MBT'$_{5Me}$ = 1 were removed as outliers. A linear correlation coefficient for all remaining samples is provided ($p << 0.01$). Sample type specific linear slopes are provided in D) with uncertainties in gray. B) Relationship between the MBT'$_{5Me}$ index and in situ temperatures for soils (blue) and cultures (pink). Shades of blue represent in situ soil temperatures averaged over different portions of the year, with abbreviations as follows: mean annual temperature (MAT), mean temperature of months above freezing (MAF), mean summer (June, July, August) temperature (JJA), and warmest month temperature (WMT). A linear correlation coefficient for cultures and soils with the WMT temperature parameter is provided ($p << 0.01$), and sample type/temperature parameter specific linear regressions are plotted in E). C) Relationship between CBT$_{5Me}$ and pH for cultures and environmental samples, with an overall linear correlation coefficient ($p << 0.01$) provided and sample type specific slopes plotted in F).*

BrGDGT Response to Temperature

Growth temperature influenced the distribution of brGDGTs produced by *S. usitatus*. An increase in methylation number, as captured by both the MBT'_{5Me} index (Fig. 2 a, b, d, e) and the Methylation (Meth) Set fractional abundances (FAs; Fig. S2), was observed at colder temperatures. These increases in methylation number occurred in parallel in acyclic and monocyclic brGDGTs (Fig. S4); fIa_{Meth} and fIb_{Meth} had a one-to-one correlation (slope = 1.00 ± 0.03) with $R^2 = 0.94$ ($p < 0.001$) across all culturing conditions in this study. All MBT'_{5Me} and Meth Set temperature relationships in culture were in good agreement with relationships observed in a wide range of environmental sample types, including soils, peats, lacustrine sediments and settling particulate matter, and marine sediments from a compiled dataset (Raberg et al., 2022b). Temperature parameters associated with these different sample types are often (necessarily) different (e.g., air temperature for soils versus sea surface temperature for marine sediments; Raberg et al., 2022a). Despite the differences in temperature sources being recorded in different brGDGT depositional environments, similarities are visible in the temperature trends represented by both the distributions of data points (Figs. 2a and S4) and linear regressions for each sample type (Figs. 2d and S5). Agreement between the temperature trends of *S. usitatus* and environmental soils was improved by the use of *in situ* soil temperatures (Fig. 2b and e) rather than the commonly used air temperatures (Fig. 2a and d). This agreement was further improved by using *in situ* soil temperatures from warmer months of the year, with the mean temperature of the warmest month providing the closest match (Figs. 2b and e and S5).

BrGDGT Response to pH

The distribution of brGDGTs produced by *S. usitatus* was affected to a lesser degree by pH. Across a pH range of 5.0-6.5, an increase in the CBT_{5Me} index was observed that was nearly orthogonal to the decreasing trends present in environmental samples (Fig. 2c and f). Examination of the Cyclization Set FAs revealed that this increase in CBT_{5Me} with pH was driven by decreasing relative abundances of cyclized compounds (Ib and IIb; Fig. S6). However, we note that these FA decreases were slight (magnitude of linear slopes < 0.7%/pH unit; Fig. S6) and that *S. usitatus*

265 cultures generally plotted within the scatter of environmental samples (Fig. S6). Due to its
266 logarithmic formulation, CBT_{5Me} is highly sensitive when the degree of brGDGT cyclization is small,
267 as was the case for *S. usitatus* cultures (Fig. S8). Therefore, the departure in the CBT_{5Me} index may
268 overemphasize small changes across a limited gradient that would be less meaningful if tested
269 across a broader range of pH. We were unable to grow *S. usitatus* outside of the 5.0-6.5 pH range
270 to further test this hypothesis.

271 **BrGDGT Response to Oxygen Limitation**

272 The brGDGT response in *S. usitatus* was tested at three levels of oxygen concentration (21%, 5%,
273 and 1% O_2). All O_2 experiments were conducted at pH 5.5 and 25°C (see Fig. 3d for experimental
274 conditions overview and growth rates). A temperature-independent methylation response was
275 observed in the 5% and 1% O_2 conditions when compared to the fully oxygenated condition (Fig.
276 3a). This methylation response is reported as % of brGDGTs (%br) (Eq. 5):

277 % of brGDGTs = [(brGDGTx) / (Ia + Ib + Ic + IIa + IIb + IIc + IIIa + IIIb + IIIc)] * 100 (Eq. 5)

278 An increase in brGDGTIIa is observed at 5% O_2 (6.1 ± 0.12 %br) relative to the 21% O_2 condition
279 (1.7 ± 0.02 %br) coupled to a decrease of brGDGTIa (92 ± 1.6 %br at 5% O_2 compared to 97 ± 2.0
280 %br at 21% O_2). In the case of the 1% O_2 condition, the percent of the membrane composed of
281 brGDGTIa is identical to the 21% O_2 condition (97%br, excluding slight offsets in error). Despite
282 the similar dominance of brGDGTIa at 1% O_2 and 21% O_2, a slight increase in the proportion of
283 brGDGTIIa to 2.8 ± 0.24 %br and a decrease in the percentage of brGDGTIIIa to 0.01% was
284 observed at 1% O_2 relative to corresponding 21% O_2 values.

285 At 1% and 5% O_2, two compounds described here as brGDGTIIIa-2 and brGDGTIIIb-2 (see
286 Fig. 1a for naming convention) were identified and structurally characterized as hexa-methylated
287 brGDGTs composed of a dimethyloctacosanyl and tetramethyloctacosanyl unit, without and with
288 an unsaturation equivalent on the tetramethyloctacosanyl unit, respectively (see Fig. 3c for
289 proposed structures, Fig. S9 for MS/MS). The abundances of these compounds in *S. usitatus* were
290 correlated with culturing O_2 (IIIa-2, R^2 = 0.96; IIIb-2, R^2 = 0.65). BrGDGTIIIa-2 increases from near-
291 zero abundance (0.08 ± .04 %br) at 21% O_2 to 2.6 ± 0.23 %br at 5% O_2) and 3.8 ± 0.39 %br at 1%

O_2. BrGDGTIIIb-2 increases from near-zero abundance (0.28 ± 0.10 %br) at 21% O_2 to 3.0 ± 0.21 %br at 5% O_2 and 1.9 ± 0.18 %br at 1% O_2 (Fig. 3b).

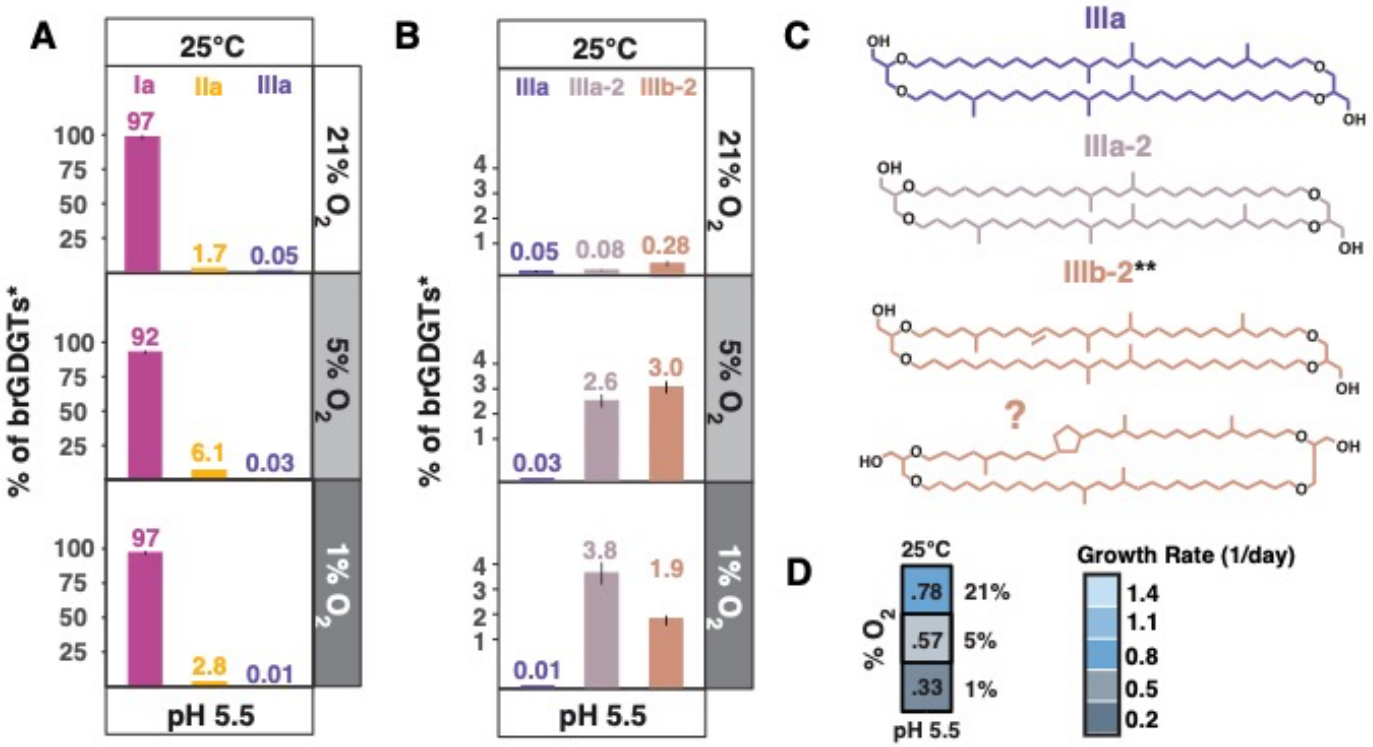

Figure 3. *Influence of oxygen concentration on brGDGT-production in S. usitatus. A) % of brGDGTs of brGDGTIa (magenta), brGDGTIIa (orange), and brGDGTIIIa (purple) at all tested oxygen concentrations. B) % of brGDGTs of brGDGTIIIa (purple), brGDGTIIIa-2 (light purple), and brGDGTIIIb-2 (brick) at all tested oxygen concentrations. C) Proposed structures of brGDGTIIIa, brGDGTIIIa-2, and brGDGTIIIb-2. D) Growth rates (1/day) of oxygen limitation experiments. *See Eq. 5 for explanation of value and note that for consistency, brGDGTIIIa-2 and brGDGTIIIb-2 are not included in the denominator. **Two structures are proposed for brGDGTIIIb-2 due to lack of MS/MS discrimination between cyclopentane rings and unsaturations.*

Discussion

Environmental relevance

While a single cultured species is unlikely to be representative of all environmentally relevant brGDGT producers, the abundance of *S. usitatus* and presently uncultured Acidobacteria with a high degree of genetic similarity to *S. usitatus* in Antarctic and Arctic soils (Pearce et al., 2012; Mannisto et al., 2007) suggests that the *Solibacter* candidate genus is an important model system for at least one group of environmentally relevant brGDGT producers. Furthermore, the agreement

310 between the response of brGDGTs to temperature in culture and in the environment may suggest
311 that membrane adaptations exhibited by *S. usitatus* are widespread in nature.

312 *S. usitatus* provides an interesting case study for understanding the purpose of brGDGT
313 production in cellular membranes. The unique properties and size of the genome of *S. usitatus*
314 provide insights into the functional modalities of this brGDGT-producing species in the environment
315 (Ward et al., 2009; Challacombe et al., 2011). *S. usitatus* has a 9.9 Mb genome, approximately 2–
316 5 times as large as other sequenced Acidobacteria genomes, and the most Sigma E homologs
317 identified in any sequenced bacterium (Challacombe et al., 2011). Sigma E regulons in bacteria
318 have been attributed to cellular stress responses such as nutrient limitation, oxidative stress, heat
319 shock, and cellular envelope stress in addition to activating outer membrane synthesis and
320 assembly (Challacombe et al., 2011; Rhodius et al., 2006; Raivio and Silhavy, 2001; Kenyon et al.,
321 2005). These genomic properties agree with the general consensus that many SD 1 and 3
322 Acidobacteria are robust oligotrophs that may have selective advantages in times of stress
323 (Eichorst et al., 2018). The physiological response of brGDGT methylation number to temperature
324 in *S. usitatus* provides insights into the competitive advantage that brGDGTs may provide to
325 oligotrophic bacteria.

326 **Implications for brGDGT-based paleoproxies**

327 We have demonstrated that relationships between brGDGTs and temperature observed widely in
328 the environment can be reproduced by a single bacterial species in culture. This observation has
329 important implications for the use of brGDGTs as a paleotemperature proxy. First, the membrane
330 restructuring exhibited by *S. usitatus* in response to temperature change supports the hypothesis
331 that methylation number plays an important role in membrane homeoviscosity, as suggested by
332 early analogies to other lipid classes (Weijers et al., 2007) and recent molecular dynamics
333 simulations (Naafs et al., 2021). Second, the co-occurrence of all major brGDGT methylation
334 numbers in *S. usitatus* provides support for the hypothesis that physiological adaptations of a
335 limited group of brGDGT producers is responsible for the distribution of the major methylated

varieties of brGDGTs in the environment as opposed to resulting solely from microbial community shifts.

Alterations to methylation number in *S. usitatus* occur in acyclic and monocyclic compounds in tandem (R^2 = 0.94; Fig. S4), further suggesting that either the enzyme responsible for C5 methylation indiscriminately methylates acyclic and monocyclic brGDGTs alike and/or that brGDGT cyclases function independently of existing C5 methylations, as has been suggested from observations in environmental samples (Raberg et al., 2021; Raberg et al., 2022a). The fact that these temperature-driven variations in brGDGT distributions are mirrored in a wide array of environmental samples (Figs. 2a, 2d, and S4) may suggest that the physiological basis for trends observed in *S. usitatus* is widespread in nature, lending confidence to the application of brGDGT-based paleotemperature proxies and encouraging their further development. For environmental soils in particular, *in situ* temperatures from the warmest portion of the year produced the closest agreement with trends observed in culture (Fig. 2 b and e). We also observed that the growth rate of *S. usitatus* was temperature-dependent, with a roughly 5-fold increase in growth rate when temperature was raised from 15 to 30°C (Fig. 1b). Growth rate was similarly observed to be exponentially dependent on temperature in lacustrine microcosm incubations (Martínez Sosa et al., 2020). Taken together, these observations suggest that the observed warm-season bias in empirical calibrations (e.g., Dearing Crampton-Flood et al., 2020) may originate from seasonal differences in bacterial growth rates. We therefore suggest a linear calibration between MBT'_{5Me} and growth temperature for use in soils,

$$\text{Growth Temperature (°C)} = 1.57 + 25.71 * MBT'_{5Me} \quad (R^2 = 0.78;\ p < 2.2e^{-16};\ n = 111) \qquad \text{(Eq. 6)}$$

where growth temperature is taken to be culturing temperature for *S. usitatus* (n = 52) and the *in situ* temperature of the warmest month for soils (n = 59). We note that while this calibration includes geographically well-distributed soils (China (Wang et al., 2020), Colombia (Pérez-Angel et al., 2020), and geothermally heated sites in Iceland (De Jonge et al., 2019), it does not include soils with warmest month temperatures below 10°C.

The relationship between brGDGTs and pH in *S. usitatus* was less pronounced than with temperature. The relative abundance of cyclized brGDGTs (Ib and IIb) in the Cyclization Set was nearly independent of pH (Fig. S6), with a slight decreasing trend (magnitude of linear slopes < 0.7%/pH unit; Fig. S7) that ran counter to the increase typically observed in environmental samples (Fig. S6) and was magnified by the logarithmic form of the CBT_{5Me} index (Fig. S8). A similar lack of pronounced pH trends was previously observed in lacustrine microcosm experiments (Martínez Sosa et al. 2020). The fact that the near-universal environment pH dependence of brGDGT cyclization number was absent or opposite in *S. usitatus* runs counter to the hypothesis that cyclizations have a direct physiological connection to pH (Weijers et al. 2007, Raberg et al. 2022a). Instead, our results may support the hypothesis that cyclization number is linked to pH via changes in bacterial community composition (De Jonge et al. 2019, De Jonge et al. 2021, Naafs et al. 2021). We note, however, that 6- and 7-methyl isomers and doubly cyclized brGDGTs were absent or nearly absent in *S. usitatus*, limiting our ability to draw comparisons with environmental samples through other pH-related indices. Furthermore, one hypothesis we present is that the numerous brGDGT isomers that are not traditionally measured in environmental samples may serve to allow *S. usitatus* to restructure its membrane in response to pH in alternative ways. Future work investigating the structural identities and response of these brGDGT isomers to culturing conditions will elucidate the role of these compounds in membrane restructuring.

Influence of Oxygen Limitation on brGDGT Production

A temperature independent methylation response was observed in the brGDGT composition of *S. usitatus* when oxygen was limited to both 5% and 1% O_2. At both low oxygen concentrations brGDGTIIa increased relative to that of the fully oxygenated experiment at the same temperature and pH conditions. However, brGDGTIIIa only increased relative to the fully oxygenated condition at 5% O_2, whereas it decreased at 1% O_2. If an increase in brGDGTIIa *and* brGDGTIIIa at suboxic conditions can be interpreted as a membrane homeostasis response to oxygen limitation in *S. usitatus*, the decrease of brGDGTIIIa at 1% O_2 relative to the fully oxygenated condition would appear to complicate this hypothesis. Although a decrease in conventional brGDGTIIIa is observed

389 at 1% O_2, an overall increase in proposed hexa-methylated compounds is observed when
390 brGDGTIIIa-2 and brGDGTIIIb-2 are considered. The presently unknown functional properties of
391 brGDGTIIIa-2 and brGDGTIIIb-2 may convey similar membrane structuring properties to
392 conventional hexa-methylated brGDGTs, thus providing support for the hypothesis that oxygen
393 limitation in *S. usitatus* results in an increase of penta- and hexa-methylated brGDGTs.

394 Although brGDGTIIIa-2 and brGDGTIIIb-2 are not regularly reported in environmental
395 studies, other similar hexa-methylated brGDGTs have previously been described from
396 environmental samples (De Jonge et al., 2013). While the previously confirmed structures of hexa-
397 methylated brGDGTs composed of a dimethyloctacosanyl and tetramethyloctacosanyl unit support
398 the interpretation of brGDGTIIIa-2 and brGDGTIIIb-2 as similar structures (Fig. 3b), our analyses
399 cannot exclude the possibility of elongated alkyl chains with fewer methyl branches generating the
400 observed m/z values of 1050 or 1048 for brGDGTIIIa-2 and brGDGTIIIb-2, respectively.

401 The production of brGDGTIIIa-2 and brGDGTIIIb-2 in *S. usitatus* under oxygen limitation
402 suggests these compounds have some potential as indicators of low oxygen in environmental
403 settings. Both brGDGTIIIa-2 and brGDGTIIIb-2 were only detected above trace levels in *S. usitatus*
404 at 5% and 1% O_2 conditions, whereas all other pH and temperature conditions tested at 21% O_2
405 yielded trace or below detection limit quantities. Determining whether brGDGTIIIa-2 and
406 brGDGTIIIb-2 are environmentally relevant is an important step for assessing their potential value
407 as a sedimentary oxygen proxy. Additionally, the overall response of environmental brGDGT
408 distributions to oxygen limitation must be resolved before brGDGTIIIa-2 and brGDGTIIIb-2 could
409 be applied to corrective measures in paleoclimate proxies.

410 Uncovering the role of oxygen limitation on brGDGT-producers *at large* is paramount to
411 ensuring the accuracy of climate records based on these compounds. Culture-based insights on
412 brGDGT response to suboxic settings are limited, but in the case of *Edaphobacter aggregans*, 1%
413 O_2 was required for the synthesis of brGDGTIa, the only conventional brGDGT identified in this
414 organism (Halamka et al., 2021). The increase in tetra-methylated brGDGTs in *E. aggregans* in
415 response to oxygen limitation conflicts with the increase in penta- and hexa-methylated brGDGTs

416 in *S. usitatus* under similar oxygen restrictions. While the enzymatic capacity of *E. aggregans* to
417 produce penta- and hexa-methylated brGDGTs remains unclear, the seemingly opposing trends in
418 methylation number response to oxygen limitation in culture serve as an important example of the
419 need to further investigate the role of oxygen in the brGDGT-producing bacterial community
420 broadly.

421 **Implications for brGDGT Biosynthesis**

422 Several lines of evidence suggest that *S. usitatus* may have a different pathway for brGDGT
423 biosynthesis than previously proposed for other Acidobacteria. Most Acidobacteria, including those
424 discovered to synthesize brGDGT Ia (Sinninghe Damsté et al., 2011), produce the membrane-
425 spanning iso-diabolic acid (iDA in Fig. 4) as a major membrane component (Sinninghe Damsté et
426 al., 2011). In addition, several Acidobacteria produce a mono-ether of iso-diabolic acid (iDA MAGE
427 in Fig. 4), which is particularly prominent in acid hydrolysis extracts from SD4 Acidobacteria and
428 occurs with additional methylations at the C5 position (Sinninghe Damsté et al., 2014). Based on
429 the abundance of these likely brGDGT precursors and the known possibility of tail-to-tail
430 condensation of fatty acids to make other membrane spanning di-acids (Fitz and Arigoni, 1992),
431 Sinninghe Damsté et al. (2011, 2014) proposed iso-diabolic acid synthesis via the condensation of
432 two iso-C15 fatty acids by a still unknown enzyme as the first step towards brGDGT synthesis (Fig.
433 4a, iso-diabolic acid pathway). The discovery of an operon for bacterial ether lipid biosynthesis (elb)
434 in myxobacteria (Lorenzen et al., 2014) then provided a potential mechanism for the conversion of
435 ester to ether bonds to form mono-, di- and eventually tetra-ethers by the ElbD enzyme as the
436 second key step of this proposed pathway (Fig. 4a), with several SD4 genomes containing
437 homologs of the entire elb operon (Sinninghe Damsté et al., 2018).

438 Contrary to most Acidobacteria studied to date, *S. usitatus* does not have detectable levels
439 of iso-diabolic acid in its cellular membrane (Table S4 and Sinninghe Damsté et al., 2018), but the
440 organism *does* produce iso-C15 mono and di-ethers (i15:0 MAGE and i15:0 DAGE in Fig. 4; Table
441 S4 and Sinninghe Damsté et al., 2018) which have been found in several other Acidobacteria as

well (Sinninghe Damsté et al., 2018). In addition, our results show that *S. usitatus* produces brGTGT (Glycerol *Tri*alkyl Glycerol Tetraethers) equivalents of all major brGDGTs (Table S3).

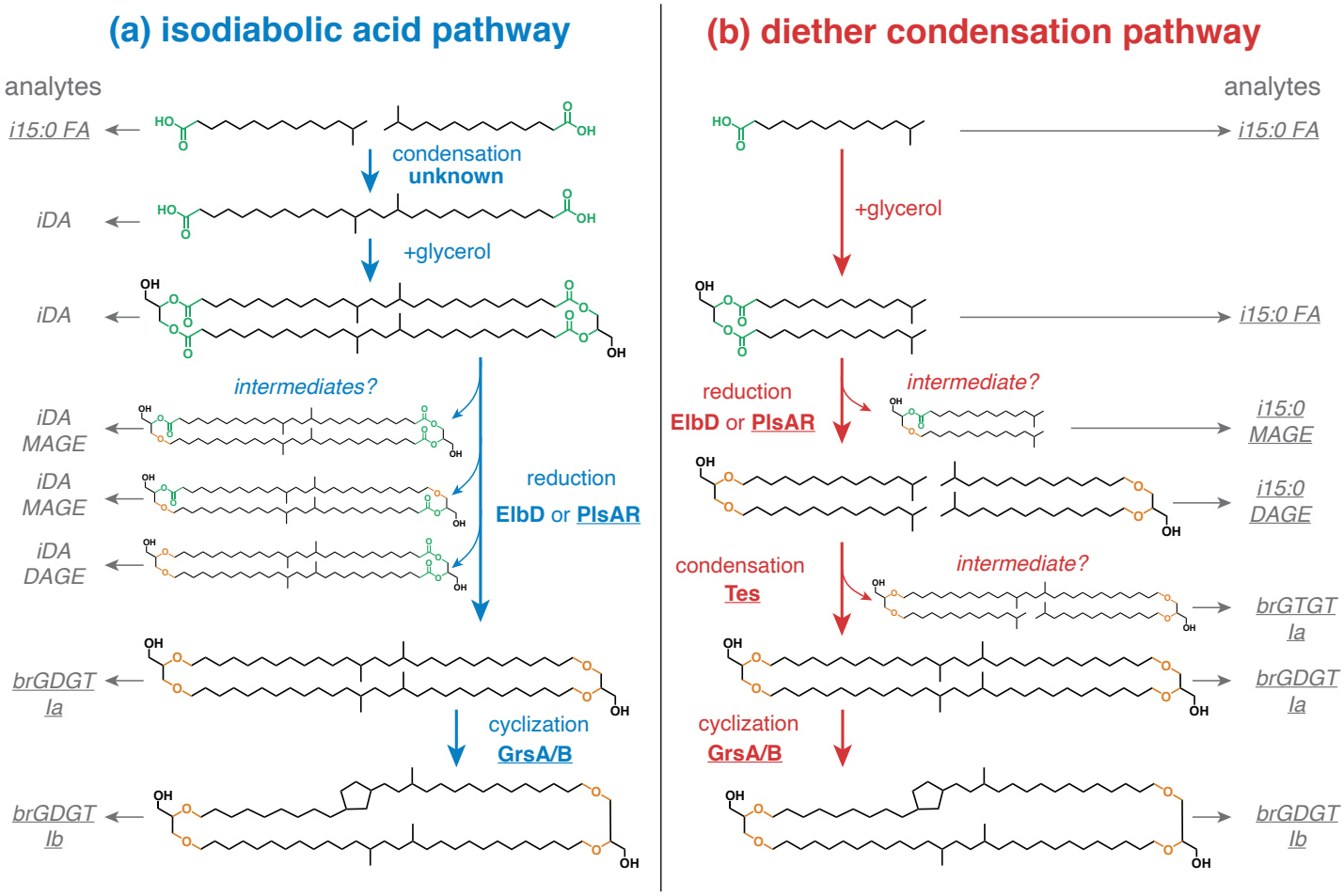

Figure 4. *Hypothesized biosynthetic pathways for brGDGT production (excluding C5/C6 methylations). A (in blue): pathway based on tail-to-tail condensation of two iso-C15:0 fatty acids to form iso-diabolic acid as a key intermediate in brGDGT biosynthesis, first proposed by Sinninghe Damsté et al. (2011, 2014, 2018). B (in red): Diether condensation pathway proposed in this study for S. usitatus based on the abundance of several potential intermediates and the existence of S. usitatus homologs of enzymes that perform similar functions in archaeal GDGTs and ester bond reduction in bacteria: Tes (tetra ether synthase), GrsA/B (GDGT ring synthesis), and PlsAR (plasmalogen synthase). Expected analytes produced by standard acid hydrolysis (which cleaves ester bonds, shown in green) for each pathway are listed on the far left and right side. Analytes that are underlined have been found in S. usitatus. Ester bonds shown in green, ether bonds shown in orange. Analytes: i15:0 FA = iso-C15:0 fatty acid; iDA = iso-diabolic acid ; iDA MAGE = 1-iso-diabolic acid monoalkanoic glycerol monoether; iDA DAGE = 1,2-iso-diabolic acid dialkanoic glycerol diether; i15:0 MAGE = 1-iso-C15:0 monoalkyl glycerol monoether; i15:0 DAGE = 1,2-iso-C15:0 dialkyl glycerol diether; brGTGT Ia = branched glycerol trialkyl glycerol tetraether.*

459 Based on these findings and the presence of several homologs of recently discovered enzymes
460 involved in ether lipid biosynthesis in bacteria and archaea (Zeng et al., 2019; Jackson et al., 2021;
461 Zeng et al., 2022), we propose an alternative pathway for brGDGT synthesis in *S. usitatus* (Fig. 4b)
462 based on tail-to-tail condensation of two iso-C15 diethers akin to the biosynthesis of isoprenoidal
463 GDGTs in Archaea (Galliker et al., 1998; Nemoto et al., 2003; Zeng et al, 2022). We hypothesize
464 that in *S. usitatus*, the conversion of ester to ether lipids is the first step towards brGDGT synthesis
465 and involves homologs of the plasmalogen ether lipid synthase PlsAR (Table S5, Fig. S10) instead
466 of ElbD, which *S. usitatus* lacks (Fig. S10). PlsAR was discovered to mediate the reduction of ester
467 to ether bonds in the anaerobic bacterial pathogen *Clostridium perfringens* (Jackson et al., 2021)
468 and has been proposed to perform a similar function in the synthesis of ether lipids in the bacterium
469 *Thermotoga maritima* (Sahonero-Canavesi et al. 2022). Next, we suggest that the condensation of
470 the resulting iso-C15 diethers is mediated by one or both *S. usitatus* homologs of the tetraether
471 synthase Tes enzyme (Fig. S10), which is involved in the synthesis of isoprenoidal GDGTs from
472 diether precursors in archaea and also produces GTGTs as potential intermediates (Zeng et al.,
473 2022). Lastly, we suggest that the homologs of the archaeal GDGT ring synthases GrsA and GrsB
474 in *S. usitatus* (Fig. S10) could be involved in the formation of pentacyclic brGDGTs akin to their
475 function in the formation of cyclized isoprenoidal GDGTs in archaea (Zeng et al., 2019).

476 Although we propose the above diether condensation pathway for *S. usitatus* (Fig. 4b)
477 based on potential intermediates and recent enzyme discoveries, it is possible that an iso-diabolic
478 acid pathway exists instead or in addition in this organism. Intermediates in biosynthetic pathways
479 only accumulate at rate-limiting steps and the findings reported in Halamka et al. (2021) suggest
480 that the abundance of iso-diabolic acid in the membrane of the SD1 Acidobacterium *E. aggregans*
481 decreases with increased brGDGT production. The apparent absence of iso-diabolic acid in *S.*
482 *usitatus* thus cannot rule out its potential role in brGDGT synthesis at a step that is not rate-limiting,
483 leading to a subsequent lack of measurable iso-diabolic, in this organism. Future work using
484 isotopic tracers *in vivo* and/or purified enzyme fractions *in vitro* has the potential to resolve the
485 exact pathway of brGDGT biosynthesis in *S. usitatus*.

Future Directions

This study demonstrates that the degree of brGDGT methylation in a single species functions as a physiological response to changing temperature, in agreement with environmental observations. The results serve as culture-based support for the use of brGDGTs as a paleothermometer, while also presenting possible caveats for the effects of O_2 on brGDGT proxies as well as new potential opportunities for identifying suboxic conditions. The results of this study do not demonstrate a clear relationship between the degree of brGDGT cyclization and pH. Instead, our findings underscore the need for further investigation into the effects of microbial community structure as well as other potential physiological factors such as growth rate, nutrient availability and carbon sources on brGDGT cyclization. Detection of brGDGTs with varying degrees of cyclization and methylation suggest that *S. usitatus* can serve as a potential genetic system to test hypotheses about the biosynthesis of brGDGTs, as well as studies on the evolutionary origin of genes involved in brGDGT synthesis in bacteria.

Acknowledgements

Shortly before the submission of this manuscript, a research team led by Zhirui Zeng submitted a manuscript describing similar findings for *S. usitatus* to the bioRxiv that independently validated many of the conclusions of this study (DOI: 10.1101/2022.04.07.487437). We reached out to Zhirui Zeng and Richard Pancost to coordinate parallel publication of our two studies and would like to thank them for their outstanding collegiality and support in this matter. We would also like to thank Stephanie Schubert, David Planck, and Nadia Dildar for laboratory assistance; Julio Sepulveda for laboratory and instrumentation access; Paula Welander and Jeremy Wei for discussions that improved this work; Bjarni Sigurdsson, Cindy de Jonge, and the Future Arctic project (MSCA-ITN-813114) for soil temperature data. This research was supported by an NSF grant (EAR 1945484) to SHK and by the University of Colorado Boulder via start-up funds and a seed grant to SHK. We acknowledge the analytical contributions of the CU Boulder Organic Geochemistry Lab (OGL) and the CU Boulder Earth Systems Stable Isotope Lab (CUBES-SIL) Core Facility

(RRID:SCR_019300). JHR acknowledges support from two NSF grants (OPP 1737712 and OPP 1836981). XLL is supported by an ACS PRF grant (61018-DNI2).

References

Barns, S. M., Cain, E. C., Sommerville, L., & Kuske, C. R. (2007). *Acidobacteria* Phylum Sequences in Uranium-Contaminated Subsurface Sediments Greatly Expand the Known Diversity within the Phylum. *Applied and Environmental Microbiology*, *73*(9), 3113–3116. https://doi.org/10.1128/AEM.02012-06

Baxter, A. J., Hopmans, E. C., Russell, J. M., & Sinninghe Damsté, J. S. (2019). Bacterial GMGTs in East African lake sediments: Their potential as palaeotemperature indicators. *Geochimica et Cosmochimica Acta*, *259*, 155–169. https://doi.org/10.1016/j.gca.2019.05.039

Challacombe, J. F., Eichorst, S. A., Hauser, L., Land, M., Xie, G., & Kuske, C. R. (2011). Biological Consequences of Ancient Gene Acquisition and Duplication in the Large Genome of Candidatus Solibacter usitatus Ellin6076. *PLoS ONE*, *6*(9), e24882. https://doi.org/10.1371/journal.pone.0024882

De Jonge, C., Hopmans, E. C., Stadnitskaia, A., Rijpstra, W. I. C., Hofland, R., Tegelaar, E., & Sinninghe Damsté, J. S. (2013). Identification of novel penta- and hexamethylated branched glycerol dialkyl glycerol tetraethers in peat using HPLC–MS2, GC–MS and GC–SMB-MS. *Organic Geochemistry*, *54*, 78–82. https://doi.org/10.1016/j.orggeochem.2012.10.004

De Jonge, C., Hopmans, E. C., Zell, C. I., Kim, J.-H., Schouten, S., & Sinninghe Damsté, J. S. (2014a). Occurrence and abundance of 6-methyl branched glycerol dialkyl glycerol tetraethers in soils: Implications for palaeoclimate reconstruction. *Geochimica et Cosmochimica Acta*, *141*, 97–112. https://doi.org/10.1016/j.gca.2014.06.013

De Jonge, C., Stadnitskaia, A., Hopmans, E. C., Cherkashov, G., Fedotov, A., & Sinninghe Damsté, J. S. (2014b). In situ produced branched glycerol dialkyl glycerol tetraethers in suspended particulate matter from the Yenisei River, Eastern Siberia. Geochimica et Cosmochimica Acta, 125, 476–491. https://doi.org/10.1016/j.gca.2013.10.031

De Jonge, C., Radujković, D., Sigurdsson, B. D., Weedon, J. T., Janssens, I., & Peterse, F. (2019). Lipid biomarker temperature proxy responds to abrupt shift in the bacterial community composition in geothermally heated soils. *Organic Geochemistry*, *137*, 103897. https://doi.org/10.1016/j.orggeochem.2019.07.006

De Jonge, C., Kuramae, E. E., Radujković, D., Weedon, J. T., Janssens, I. A., & Peterse, F. (2021). The influence of soil chemistry on branched tetraether lipids in mid- and high latitude soils: Implications for brGDGT- based paleothermometry. Geochimica et Cosmochimica Acta, 310, 95–112. https://doi.org/10.1016/j.gca.2021.06.037

Dearing Crampton-Flood, E., Noorbergen, L. J., Smits, D., Boschman, R. C., Donders, T. H., Munsterman, D. K., ten Veen, J., Peterse, F., Lourens, L., & Sinninghe Damsté, J. S. (2020). A new age model for the Pliocene of the southern North Sea basin: A multi-proxy climate reconstruction. *Climate of the Past*, *16*(2), 523–541. https://doi.org/10.5194/cp-16-523-2020

Eichorst, S. A., Trojan, D., Roux, S., Herbold, C., Rattei, T., & Woebken, D. (2018). Genomic insights into the *Acidobacteria* reveal strategies for their success in terrestrial environments. *Environmental Microbiology*, *20*(3), 1041–1063. https://doi.org/10.1111/1462-2920.14043

Fitz, W., & Arigoni, D. (1992). Biosynthesis of 15,16-dimethyltriacontanedioic acid (diabolic acid) from [16-2H3]- and [14-2H2]-palmitic acids. Journal of the Chemical Society, Chemical Communications, 20, 1533. https://doi.org/10.1039/c39920001533

Galliker, P., Grather, O., Riimmler, M., Fitz, W. and Arigoni, D. (1998). New Structural and Biosynthetic Aspects of the Unusual Core Lipids from Archaebacteria. In Vitamin B12 and B12-Proteins (eds B. Kräutler, D. Arigoni and B.T. Golding). https://doi.org/10.1002/9783527612192.ch29

George, I. F., Hartmann, M., Liles, M. R., & Agathos, S. N. (2011). Recovery of As-Yet-Uncultured Soil Acidobacteria on Dilute Solid Media. *Applied and Environmental Microbiology*, *77*(22), 8184–8188. https://doi.org/10.1128/AEM.05956-11

Guo, J., Ma, T., Liu, N., Zhang, X., Hu, H., Ma, W., Wang, Z., Feng, X., & Peterse, F. (2022). Soil pH and aridity influence distributions of branched tetraether lipids in grassland soils along an aridity transect. *Organic Geochemistry*, *164*, 104347. https://doi.org/10.1016/j.orggeochem.2021.104347

Halamka, T. A., McFarlin, J. M., Younkin, A. D., Depoy, J., Dildar, N., & Kopf, S. H. (2021). Oxygen limitation can trigger the production of branched GDGTs in culture. *Geochemical Perspectives Letters*, 36–39. https://doi.org/10.7185/geochemlet.2132

Halffman, R., Lembrechts, J., Radujković, D., De Gruyter, J., Nijs, I., & De Jonge, C. (2022). Soil chemistry, temperature and bacterial community composition drive brGDGT distributions along a subarctic elevation gradient. *Organic Geochemistry*, *163*, 104346. https://doi.org/10.1016/j.orggeochem.2021.104346

Hopmans, E. C., Weijers, J. W. H., Schefuß, E., Herfort, L., Sinninghe Damsté, J. S., & Schouten, S. (2004). A novel proxy for terrestrial organic matter in sediments based on branched and isoprenoid tetraether lipids. Earth and Planetary Science Letters, 224(1–2), 107–116. https://doi.org/10.1016/j.epsl.2004.05.012

Hopmans, E. C., Schouten, S., & Sinninghe Damsté, J. S. (2016). The effect of improved chromatography on GDGT-based palaeoproxies. *Organic Geochemistry*, *93*, 1–6. https://doi.org/10.1016/j.orggeochem.2015.12.006

Huguet, C., Hopmans, E. C., Febo-Ayala, W., Thompson, D. H., Sinninghe Damsté, J. S., & Schouten, S. (2006). An improved method to determine the absolute abundance of glycerol dibiphytanyl glycerol tetraether lipids. *Organic Geochemistry*, *37*(9), 1036–1041. https://doi.org/10.1016/j.orggeochem.2006.05.008

Hunter, S., Apweiler, R., Attwood, T. K., Bairoch, A., Bateman, A., Binns, D., Bork, P., Das, U., Daugherty, L., Duquenne, L., Finn, R. D., Gough, J., Haft, D., Hulo, N., Kahn, D., Kelly, E., Laugraud, A., Letunic, I., Lonsdale, D., … Yeats, C. (2009). InterPro: The integrative protein signature database. *Nucleic Acids Research*, *37*(Database), D211–D215. https://doi.org/10.1093/nar/gkn785

Jackson, D. R., Cassilly, C. D., Plichta, D. R., Vlamakis, H., Liu, H., Melville, S. B., Xavier, R. J., & Clardy, J. (2021). Plasmalogen Biosynthesis by Anaerobic Bacteria: Identification of a Two-Gene Operon Responsible for Plasmalogen Production in *Clostridium perfringens*. *ACS Chemical Biology*, *16*(1), 6–13. https://doi.org/10.1021/acschembio.0c00673

Jones, R. T., Robeson, M. S., Lauber, C. L., Hamady, M., Knight, R., & Fierer, N. (2009). A comprehensive survey of soil acidobacterial diversity using pyrosequencing and clone library analyses. *The ISME Journal*, *3*(4), 442–453. https://doi.org/10.1038/ismej.2008.127

Joseph, S. J., Hugenholtz, P., Sangwan, P., Osborne, C. A., & Janssen, P. H. (2003). Laboratory Cultivation of Widespread and PreviouslyUncultured SoilBacteria. *Applied and Environmental Microbiology*, *69*(12), 7210–7215. https://doi.org/10.1128/AEM.69.12.7210-7215.2003

Kenyon, W. J., Thomas, S. M., Johnson, E., Pallen, M. J., & Spector, M. P. (2005). Shifts from glucose to certain secondary carbon-sources result in activation of the extracytoplasmic function sigma factor σ E in Salmonella enterica serovar Typhimurium. *Microbiology*, *151*(7), 2373–2383. https://doi.org/10.1099/mic.0.27649-0

Lauretano, V., Kennedy-Asser, A. T., Korasidis, V. A., Wallace, M. W., Valdes, P. J., Lunt, D. J., Pancost, R. D., & Naafs, B. D. A. (2021). Eocene to Oligocene terrestrial Southern Hemisphere cooling caused by declining pCO2. *Nature Geoscience*, *14*(9), 659–664. https://doi.org/10.1038/s41561-021-00788-z

Lincoln, S. A., Bradley, A. S., Newman, S. A., & Summons, R. E. (2013). Archaeal and bacterial glycerol dialkyl glycerol tetraether lipids in chimneys of the Lost City Hydrothermal Field. *Organic Geochemistry*, *60*, 45–53. https://doi.org/10.1016/j.orggeochem.2013.04.010

Lindberg, K. R., Daniels, W. C., Castañeda, I. S., & Brigham-Grette, J. (2022). Biomarker proxy records of Arctic climate change during the Mid-Pleistocene transition from Lake El'gygytgyn (Far East Russia). Climate of the Past, 18(3), 559–577. https://doi.org/10.5194/cp-18-559-2022

Liu, X.-L., Zhu, C., Wakeham, S. G., & Hinrichs, K.-U. (2014). In situ production of branched glycerol dialkyl glycerol tetraethers in anoxic marine water columns. *Marine Chemistry*, *166*, 1–8. https://doi.org/10.1016/j.marchem.2014.08.008

Liu, X.-L., Russell, D. A., Bonfio, C., & Summons, R. E. (2019). Glycerol configurations of environmental GDGTs investigated using a selective sn2 ether cleavage protocol. Organic Geochemistry, 128, 57–62. https://doi.org/10.1016/j.orggeochem.2018.12.003

Lorenzen, W., Ahrendt, T., Bozhüyük, K. A. J., & Bode, H. B. (2014). A multifunctional enzyme is involved in bacterial ether lipid biosynthesis. *Nature Chemical Biology*, *10*(6), 425–427. https://doi.org/10.1038/nchembio.1526

Lu, H., Liu, W., Yang, H., Wang, H., Liu, Z., Leng, Q., Sun, Y., Zhou, W., & An, Z. (2019). 800-kyr land temperature variations modulated by vegetation changes on Chinese Loess Plateau. *Nature Communications*, *10*(1), 1958. https://doi.org/10.1038/s41467-019-09978-1

Mannisto, M. K., Tiirola, M., & Haggblom, M. M. (2007). Bacterial communities in Arctic fjelds of Finnish Lapland are stable but highly pH-dependent: Bacterial communities in Arctic fjelds of Finnish Lapland. *FEMS Microbiology Ecology*, *59*(2), 452–465. https://doi.org/10.1111/j.1574-6941.2006.00232.x

Martínez-Sosa, P., & Tierney, J. E. (2019). Lacustrine brGDGT response to microcosm and mesocosm incubations. *Organic Geochemistry*, *127*, 12–22. https://doi.org/10.1016/j.orggeochem.2018.10.011

Martínez-Sosa, P., Tierney, J. E., & Meredith, L. K. (2020). Controlled lacustrine microcosms show a brGDGT response to environmental perturbations. *Organic Geochemistry*, *145*, 104041. https://doi.org/10.1016/j.orggeochem.2020.104041

Martínez-Sosa, P., Tierney, J. E., Stefanescu, I. C., Dearing Crampton-Flood, E., Shuman, B. N., & Routson, C. (2021). A global Bayesian temperature calibration for lacustrine brGDGTs. *Geochimica et Cosmochimica Acta*, *305*, 87–105. https://doi.org/10.1016/j.gca.2021.04.038

Naafs, B. D. A., Gallego-Sala, A. V., Inglis, G. N., & Pancost, R. D. (2017b). Refining the global branched glycerol dialkyl glycerol tetraether (brGDGT) soil temperature calibration. *Organic Geochemistry*, *106*, 48–56. https://doi.org/10.1016/j.orggeochem.2017.01.009

Naafs, B. D. A., Inglis, G. N., Zheng, Y., Amesbury, M. J., Biester, H., Bindler, R., Blewett, J., Burrows, M. A., del Castillo Torres, D., Chambers, F. M., Cohen, A. D., Evershed, R. P., Feakins, S. J., Gałka, M., Gallego-Sala, A., Gandois, L., Gray, D. M., Hatcher, P. G., Honorio Coronado, E. N., … Pancost, R. D. (2017a). Introducing global peat-specific temperature and pH calibrations based on brGDGT bacterial lipids. *Geochimica et Cosmochimica Acta*, *208*, 285–301. https://doi.org/10.1016/j.gca.2017.01.038

Naafs, B. D. A., Oliveira, A. S. F., & Mulholland, A. J. (2021). Molecular dynamics simulations support the hypothesis that the brGDGT paleothermometer is based on homeoviscous

adaptation. *Geochimica et Cosmochimica Acta*, *312*, 44–56. https://doi.org/10.1016/j.gca.2021.07.034

Nemoto, N., Shida, Y., Shimada, H., Oshima, T., & Yamagishi, A. (2003). Characterization of the precursor of tetraether lipid biosynthesis in the thermoacidophilic archaeon Thermoplasma acidophilum. Extremophiles, 7(3), 235–243. https://doi.org/10.1007/s00792-003-0315-x

Pearce, D. A., Newsham, K. K., Thorne, M. A. S., Calvo-Bado, L., Krsek, M., Laskaris, P., Hodson, A., & Wellington, E. M. (2012). Metagenomic Analysis of a Southern Maritime Antarctic Soil. *Frontiers in Microbiology*, *3*. https://doi.org/10.3389/fmicb.2012.00403

Pérez-Angel, L. C., Sepúlveda, J., Molnar, P., Montes, C., Rajagopalan, B., Snell, K., Gonzalez-Arango, C., & Dildar, N. (2020). Soil and Air Temperature Calibrations Using Branched GDGTs for the Tropical Andes of Colombia: Toward a Pan-Tropical Calibration. *Geochemistry, Geophysics, Geosystems*, *21*(8). https://doi.org/10.1029/2020GC008941

Peterse, F., van der Meer, J., Schouten, S., Weijers, J. W. H., Fierer, N., Jackson, R. B., Kim, J.-H., & Sinninghe Damsté, J. S. (2012). Revised calibration of the MBT–CBT paleotemperature proxy based on branched tetraether membrane lipids in surface soils. *Geochimica et Cosmochimica Acta*, *96*, 215–229. https://doi.org/10.1016/j.gca.2012.08.011

Raberg, J. H., Harning, D. J., Crump, S. E., de Wet, G., Blumm, A., Kopf, S., Geirsdóttir, Á., Miller, G. H., & Sepúlveda, J. (2021). Revised fractional abundances and warm-season temperatures substantially improve brGDGT calibrations in lake sediments. *Biogeosciences*, *18*(12), 3579–3603. https://doi.org/10.5194/bg-18-3579-2021

Raberg J. H., Miller G. H., Geirsdóttir Á. and Sepúlveda J. (2022a) [in press], Near-universal trends in brGDGT lipid distributions in nature.

Raberg, Jonathan H; Miller, Gifford H; Geirsdóttir, Áslaug; Sepúlveda, Julio (2022b): Global compilation of brGDGT lipid distributions, temperature, and pH across a dozen sample types. PANGAEA, https://doi.org/10.1594/PANGAEA.940052

Raivio, T. L., & Silhavy, T. J. (2001). Periplasmic Stress and ECF Sigma Factors. *Annual Review of Microbiology*, *55*(1), 591–624. https://doi.org/10.1146/annurev.micro.55.1.591

Rhodius, V. A., Suh, W. C., Nonaka, G., West, J., & Gross, C. A. (2005). Conserved and Variable Functions of the σE Stress Response in Related Genomes. *PLoS Biology*, *4*(1), e2. https://doi.org/10.1371/journal.pbio.0040002

Sahonero-Canavesi, D. X., Villanueva, L., Bale, N. J., Bosviel, J., Koenen, M., Hopmans, E. C., & Sinninghe Damsté, J. S. (2022). Changes in the Distribution of Membrane Lipids during Growth of Thermotoga maritima at Different Temperatures: Indications for the Potential Mechanism of Biosynthesis of Ether-Bound Diabolic Acid (Membrane-Spanning) Lipids. *Applied and Environmental Microbiology*, *88*(2), e01763-21. https://doi.org/10.1128/AEM.01763-21

Sigurdsson, B. D., Leblans, N. I. W., Dauwe, S., Guðmundsdóttir, E., Gundersen, P., Gunnarsdóttir, G. E., Holmstrup, M., Ilieva-Makulec, K., Kätterer, T., Marteinsdóttir, B., Maljanen, M., Oddsdóttir, E. S., Ostonen, I., Peñuelas, J., Poeplau, C., Richter, A., Sigurðsson, P., van Bodegom, P., Wallander, H., … Janssens, I. (2016). Geothermal ecosystems as natural climate change experiments: The ForHot research site in Iceland as a case study. *Icelandic Agricultural Sciences*, *29*, 53–71. https://doi.org/10.16886/IAS.2016.05

Sinninghe Damsté, J. S., Rijpstra, W. I. C., Foesel, B. U., Huber, K. J., Overmann, J., Nakagawa, S., Kim, J. J., Dunfield, P. F., Dedysh, S. N., & Villanueva, L. (2018). An overview of the occurrence of ether- and ester-linked iso-diabolic acid membrane lipids in microbial cultures of the Acidobacteria: Implications for brGDGT paleoproxies for temperature and pH. *Organic Geochemistry*, *124*, 63–76. https://doi.org/10.1016/j.orggeochem.2018.07.006

Sinninghe Damsté, J. S., Rijpstra, W. I. C., Hopmans, E. C., Foesel, B. U., Wüst, P. K., Overmann, J., Tank, M., Bryant, D. A., Dunfield, P. F., Houghton, K., & Stott, M. B. (2014). Ether- and Ester-Bound *iso* -Diabolic Acid and Other Lipids in Members of Acidobacteria Subdivision 4. *Applied and Environmental Microbiology*, *80*(17), 5207–5218. https://doi.org/10.1128/AEM.01066-14

Sinninghe Damsté, J. S., Rijpstra, W. I. C., Hopmans, E. C., Weijers, J. W. H., Foesel, B. U., Overmann, J., & Dedysh, S. N. (2011). 13,16-Dimethyl Octacosanedioic Acid (iso -Diabolic Acid), a Common Membrane-Spanning Lipid of Acidobacteria Subdivisions 1 and 3. *Applied and Environmental Microbiology*, *77*(12), 4147–4154. https://doi.org/10.1128/AEM.00466-11

Sinninghe Damsté, J. S., Hopmans, E. C., Pancost, R. D., Schouten, S., & Geenevasen, J. A. J. (2000). Newly discovered non-isoprenoid glycerol dialkyl glycerol tetraether lipids in sediments. *Chemical Communications*, *17*, 1683–1684. https://doi.org/10.1039/b004517i

Tierney, J. E., & Russell, J. M. (2009). Distributions of branched GDGTs in a tropical lake system: Implications for lacustrine application of the MBT/CBT paleoproxy. Organic Geochemistry, 40(9), 1032–1036. https://doi.org/10.1016/j.orggeochem.2009.04.014

Wang, H., An, Z., Lu, H., Zhao, Z., & Liu, W. (2020). Calibrating bacterial tetraether distributions towards in situ soil temperature and application to a loess-paleosol sequence. *Quaternary Science Reviews*, *231*, 106172. https://doi.org/10.1016/j.quascirev.2020.106172

Wang, H., & Liu, W. (2021). Soil temperature and brGDGTs along an elevation gradient on the northeastern Tibetan Plateau: A test of soil brGDGTs as a proxy for paleoelevation. *Chemical Geology*, *566*, 120079. https://doi.org/10.1016/j.chemgeo.2021.120079

Wang, H., Liu, W., He, Y., Zhou, A., Zhao, H., Liu, H., Cao, Y., Hu, J., Meng, B., Jiang, J., Kolpakova, M., Krivonogov, S., & Liu, Z. (2021). Salinity-controlled isomerization of lacustrine brGDGTs impacts the associated M B T 5 M E ' terrestrial temperature index. *Geochimica et Cosmochimica Acta*, *305*, 33–48. https://doi.org/10.1016/j.gca.2021.05.004

Wang, M., Zheng, Z., Zong, Y., Man, M., & Tian, L. (2019). Distributions of soil branched glycerol dialkyl glycerol tetraethers from different climate regions of China. *Scientific Reports*, *9*(1), 2761. https://doi.org/10.1038/s41598-019-39147-9

Ward, N. L., Challacombe, J. F., Janssen, P. H., Henrissat, B., Coutinho, P. M., Wu, M., Xie, G., Haft, D. H., Sait, M., Badger, J., Barabote, R. D., Bradley, B., Brettin, T. S., Brinkac, L. M., Bruce, D., Creasy, T., Daugherty, S. C., Davidsen, T. M., DeBoy, R. T., … Kuske, C. R. (2009). Three Genomes from the Phylum *Acidobacteria* Provide Insight into the Lifestyles of These Microorganisms in Soils. *Applied and Environmental Microbiology*, *75*(7), 2046–2056. https://doi.org/10.1128/AEM.02294-08

Weber, Y., Sinninghe Damsté, J. S., Zopfi, J., De Jonge, C., Gilli, A., Schubert, C. J., Lepori, F., Lehmann, M. F., & Niemann, H. (2018). Redox-dependent niche differentiation provides evidence for multiple bacterial sources of glycerol tetraether lipids in lakes. *Proceedings of the National Academy of Sciences*, *115*(43), 10926–10931. https://doi.org/10.1073/pnas.1805186115

Weijers, J. W. H., Panoto, E., van Bleijswijk, J., Schouten, S., Rijpstra, W. I. C., Balk, M., Stams, A. J. M., & Damsté, J. S. S. (2009). Constraints on the Biological Source(s) of the Orphan Branched Tetraether Membrane Lipids. *Geomicrobiology Journal*, *26*(6), 402–414. https://doi.org/10.1080/01490450902937293

Weijers, J. W. H., Schouten, S., Hopmans, E. C., Geenevasen, J. A. J., David, O. R. P., Coleman, J. M., Pancost, R. D., & Sinninghe Damste, J. S. (2006). Membrane lipids of mesophilic anaerobic bacteria thriving in peats have typical archaeal traits. *Environmental Microbiology*, *8*(4), 648–657. https://doi.org/10.1111/j.1462-2920.2005.00941.x

Weijers, J. W. H., Schouten, S., van den Donker, J. C., Hopmans, E. C., & Sinninghe Damsté, J. S. (2007). Environmental controls on bacterial tetraether membrane lipid distribution in soils. *Geochimica et Cosmochimica Acta*, *71*(3), 703–713. https://doi.org/10.1016/j.gca.2006.10.003

Weijers, J. W. H., Wiesenberg, G. L. B., Bol, R., Hopmans, E. C., & Pancost, R. D. (2010). Carbon isotopic composition of branched tetraether membrane lipids in soils suggest a rapid turnover and a heterotrophic life style of their source organism(s). *Biogeosciences*, *7*(9), 2959–2973. https://doi.org/10.5194/bg-7-2959-2010

Wu, J., Yang, H., Pancost, R. D., Naafs, B. D. A., Qian, S., Dang, X., Sun, H., Pei, H., Wang, R., Zhao, S., & Xie, S. (2021). Variations in dissolved O2 in a Chinese lake drive changes in microbial communities and impact sedimentary GDGT distributions. *Chemical Geology*, *579*, 120348. https://doi.org/10.1016/j.chemgeo.2021.120348

Xiao, W., Xu, Y., Lin, J., Zeng, Z., Liu, Y., Zhang, H., & Zhang, C. (2022). Global scale production of brGDGTs by benthic marine bacteria: Implication for developing ocean bottom

environmental proxies. Global and Planetary Change, 211, 103783. https://doi.org/10.1016/j.gloplacha.2022.103783

Zeng, Z., Chen, H., Yang, H., Chen, Y., Yang, W., Feng, X., Pei, H., & Welander, P. V. (2022). Identification of a protein responsible for the synthesis of archaeal membrane-spanning GDGT lipids. *Nature Communications*, *13*(1), 1545. https://doi.org/10.1038/s41467-022-29264-x

Zeng, Z., Liu, X.-L., Farley, K. R., Wei, J. H., Metcalf, W. W., Summons, R. E., & Welander, P. V. (2019). GDGT cyclization proteins identify the dominant archaeal sources of tetraether lipids in the ocean. *Proceedings of the National Academy of Sciences*, *116*(45), 22505–22511. https://doi.org/10.1073/pnas.1909306116

Supplementary Figures

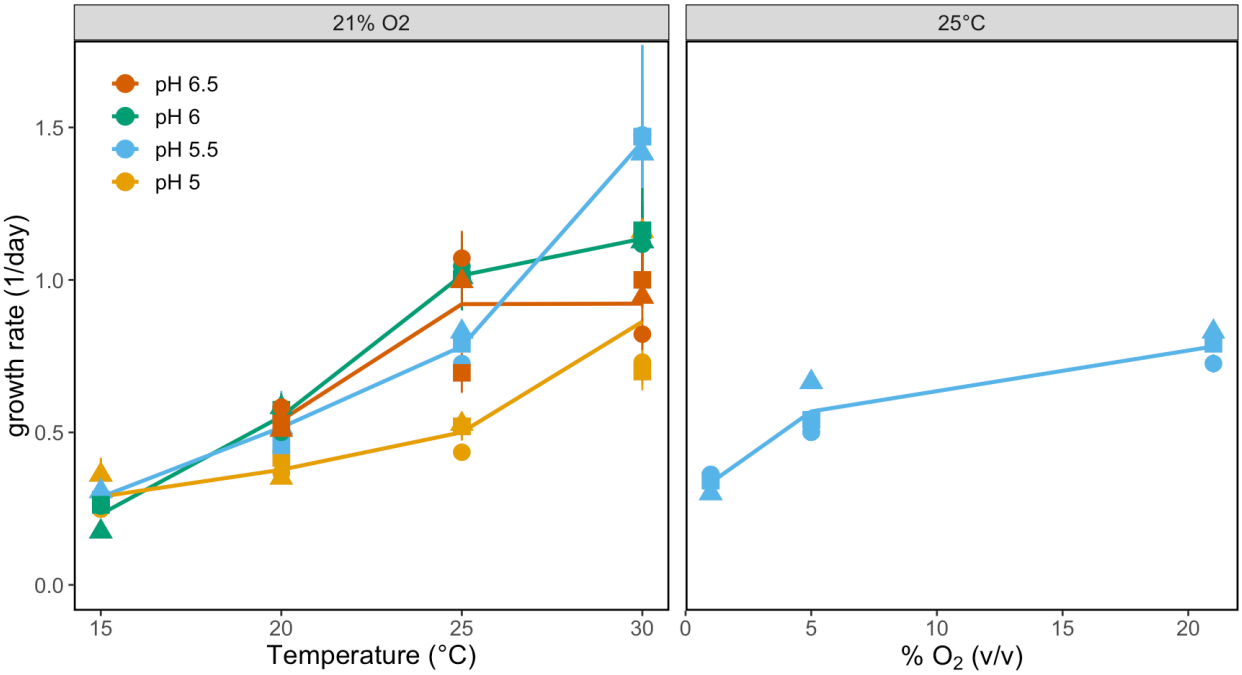

Fig. S1. Growth rates of *S. usitatus* at different oxygen concentrations, temperatures and pH. Shapes differentiate replicate cultures. Error bars indicate standard errors of growth rate estimates from regression fits. Some error bars are smaller than symbol sizes. See Table S2 for all numerical values.

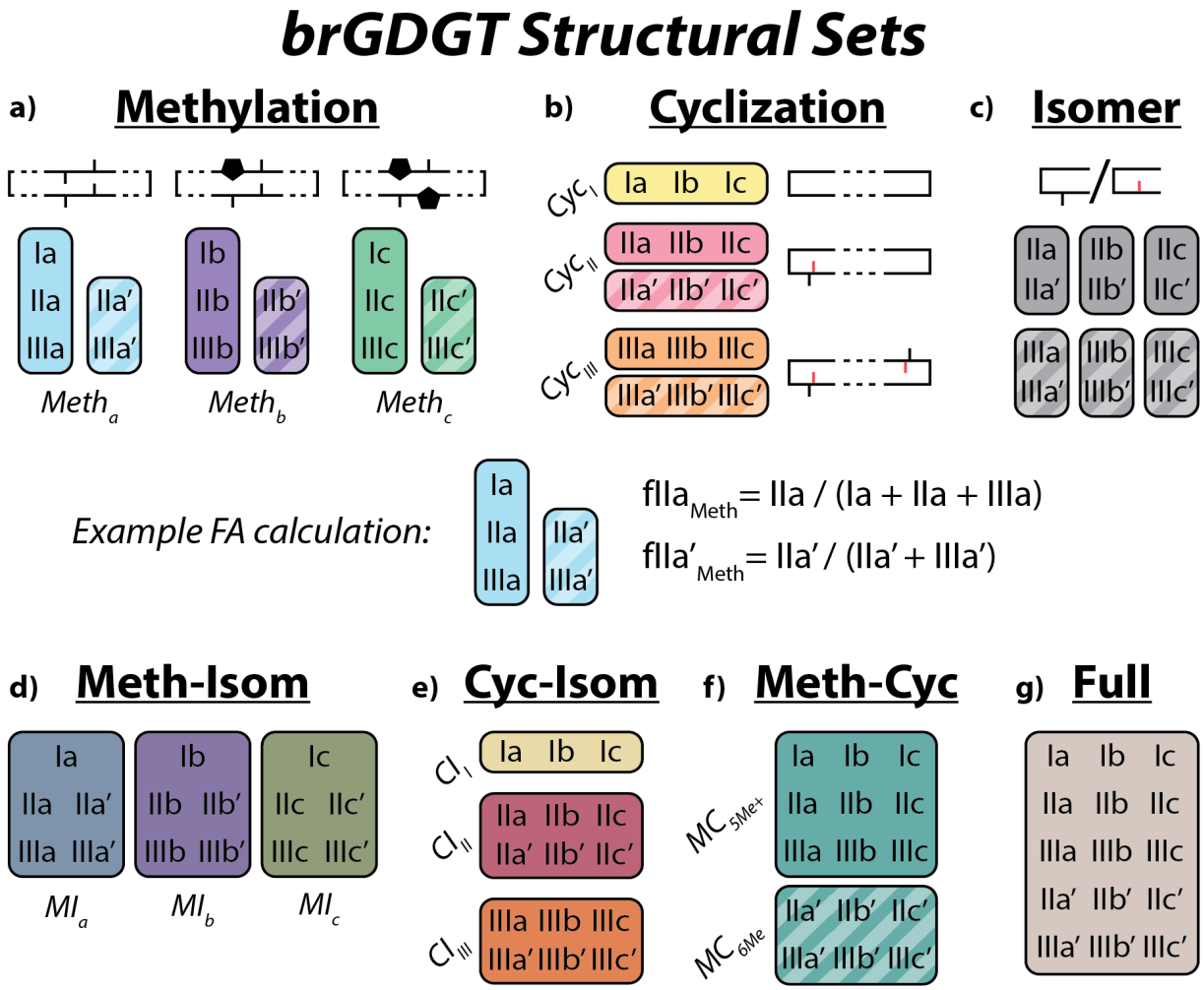

Fig. S2. Schematic of the basic (a-c) and combined (d-g) brGDGT structural sets. Fractional abundances are calculated within each boxed group independently (example calculation in center). Schematic structures highlight the defining alkyl-chain moieties, with cyclopentane rings filled in for emphasis and C6 methylations denoted in red. (Reproduced from Raberg et al. (2021)).

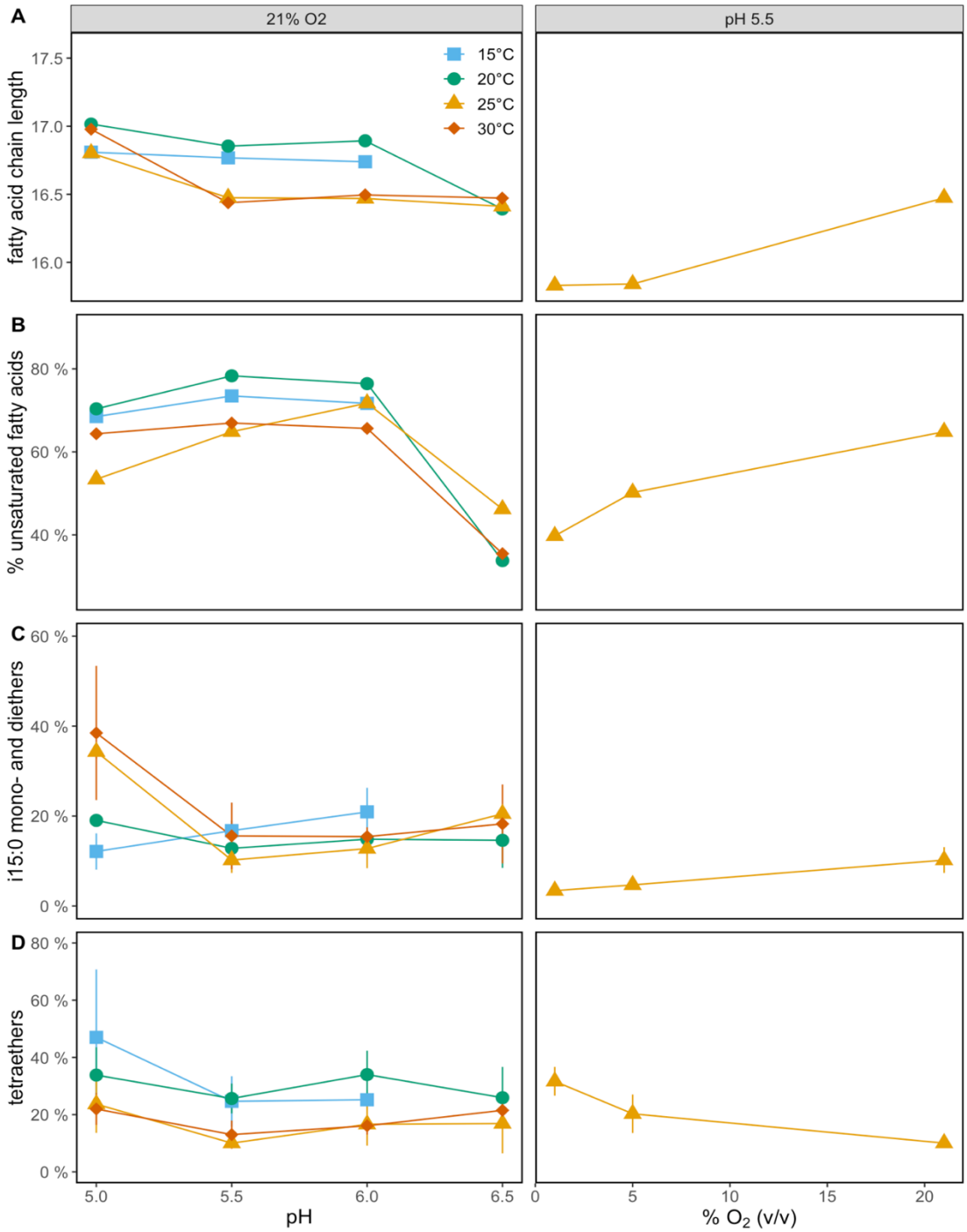

Fig. S3. Lipid abundance patterns of *S. usitatus* across all experiments vs pH at 21% O_2 on the left and vs. %O_2 at pH 5.5 on the right. (a) weighted average carbon chain length of all fatty acids. (b) weighted average unsaturation of all fatty acids. (c) overall abundance of mono and diethers. (d) overall abundance of tetraethers. See Tables S1 and S3 for underlying data.

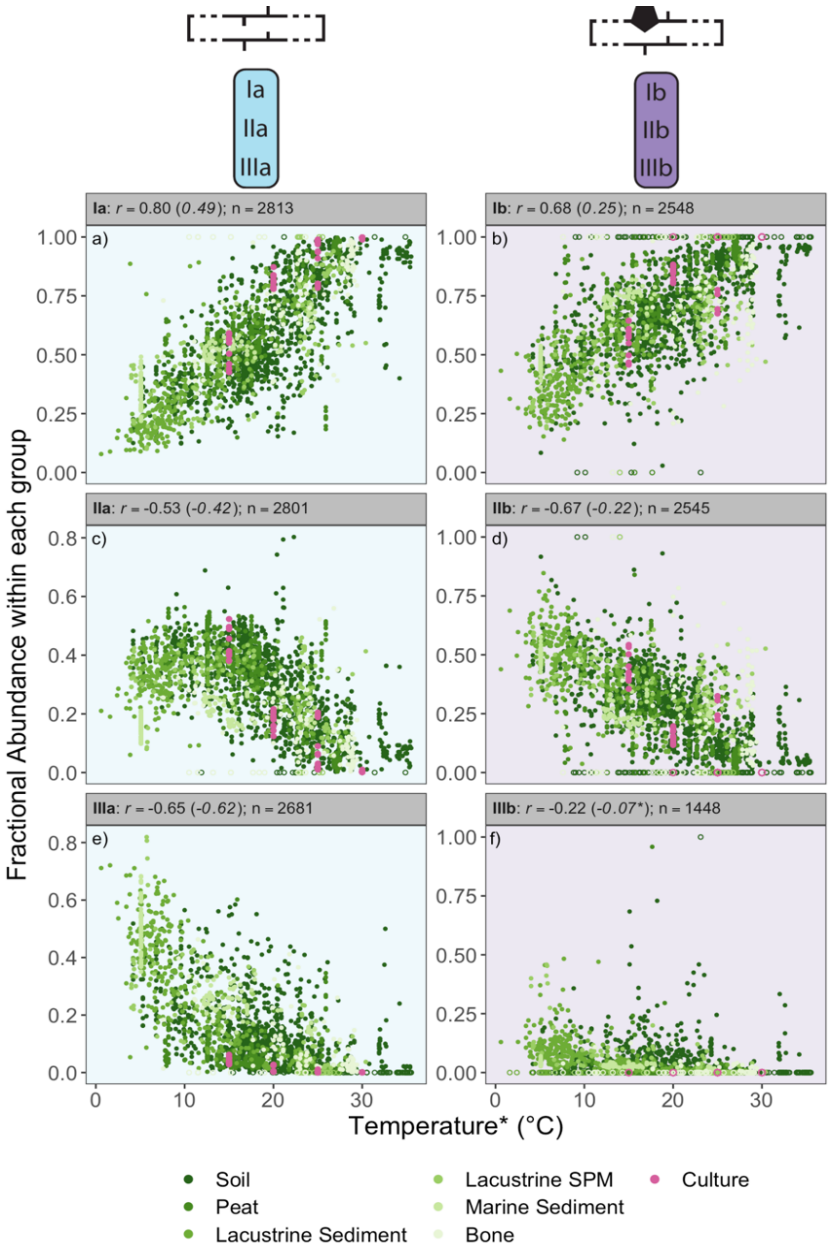

Fig. S4. Relationship between Methylation Set fractional abundances (FAs) of 5-methyl acyclic and monocyclic brGDGTs and temperature. Linear correlation coefficients *r* across *n* samples are provided for each subplot, with coefficients for the standard Full FAs given in parentheses for comparison. P values were <0.01 except where marked with an asterisk. Samples with FA = 0 or 1 were treated as outliers and removed from statistical analyses (*r*, *n,* and p values). *Temperatures were associated with different sample types following Raberg et al. (2022a). Schematics of Methylation Set groupings are provided at top.

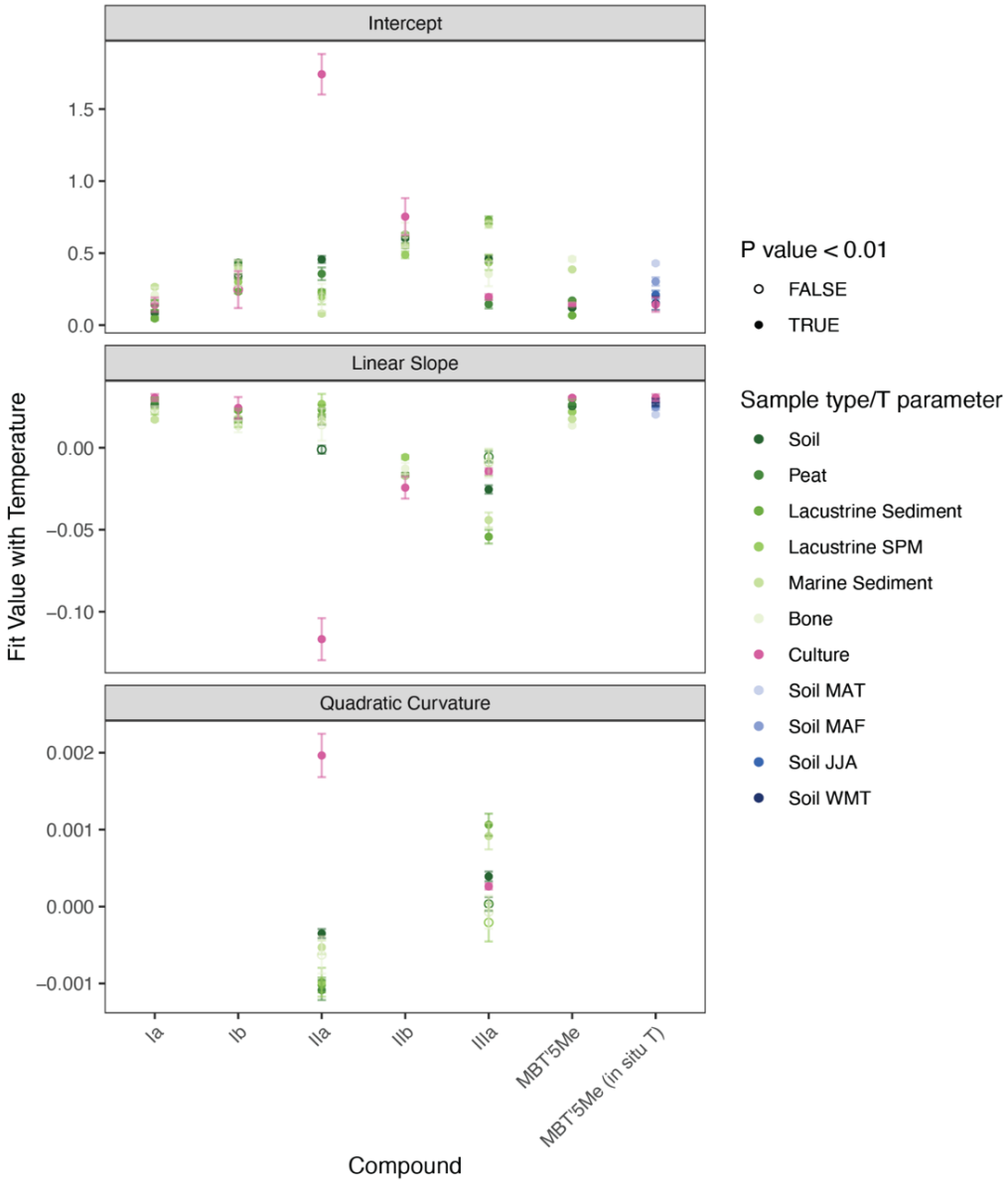

Fig. S5. Fitting coefficients for quadratic (IIa and IIIa) and linear (all others) regressions between brGDGT Methylation Set fractional abundances, MBT'$_{5Me}$ and temperature, as plotted in Figures S4 and 2D, as well as between MBT'$_{5Me}$ and *in situ* temperature as plotted in Figure 2E. Error bars represent one standard error. Coefficients with p values ≥ 0.01 are plotted as open circles. Abbreviations are defined in Figure 2 caption.

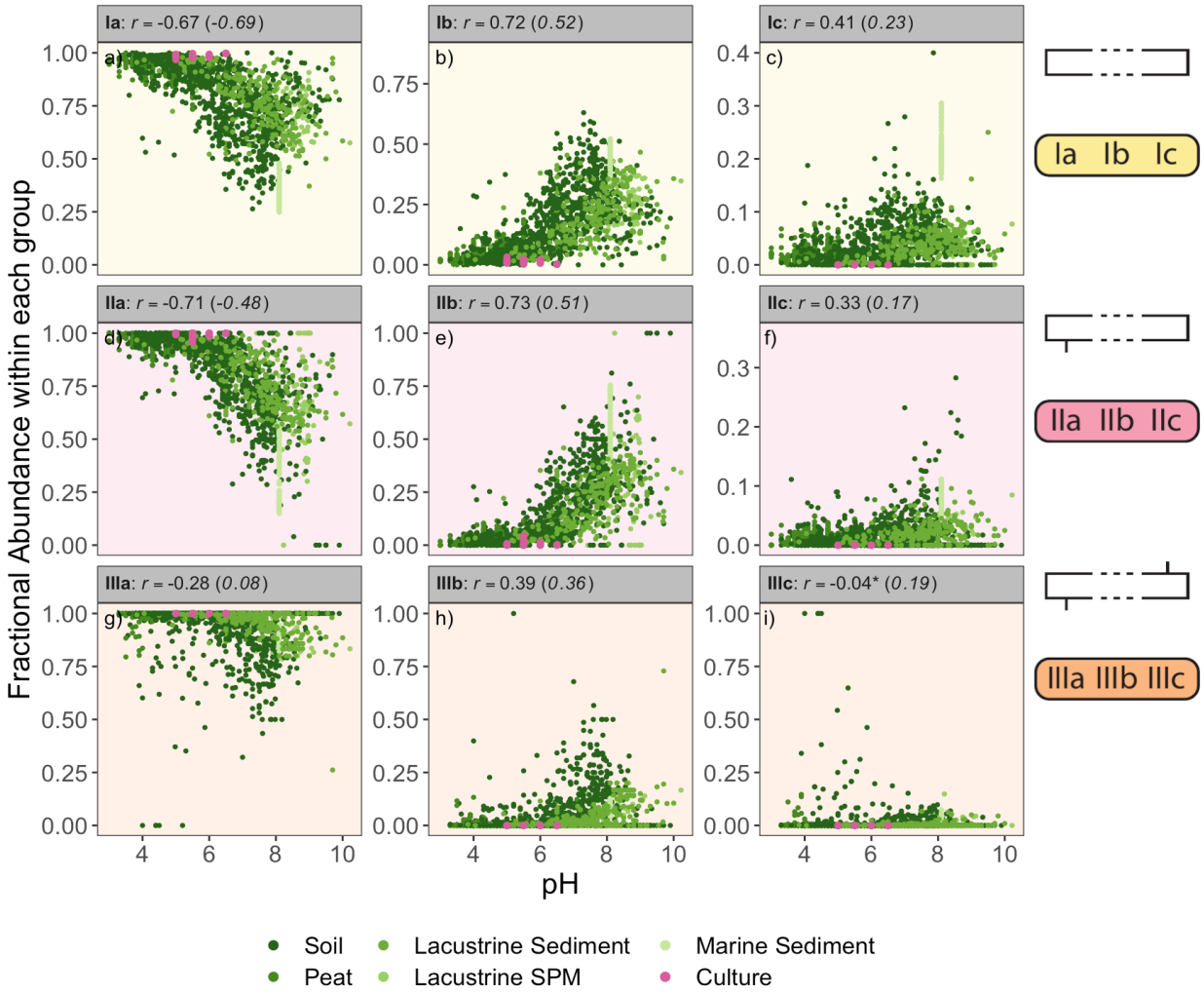

Fig. S6. Relationship between Cyclization Set fractional abundances (FAs) of 5-methyl brGDGTs and pH. Linear correlation coefficients *r* are provided for each subplot (*n* = 1856 for all), with coefficients for the standard Full FAs given in parentheses for comparison. P values were <0.01 except where marked with an asterisk. Schematics of Cyclization Set groupings are provided at right.

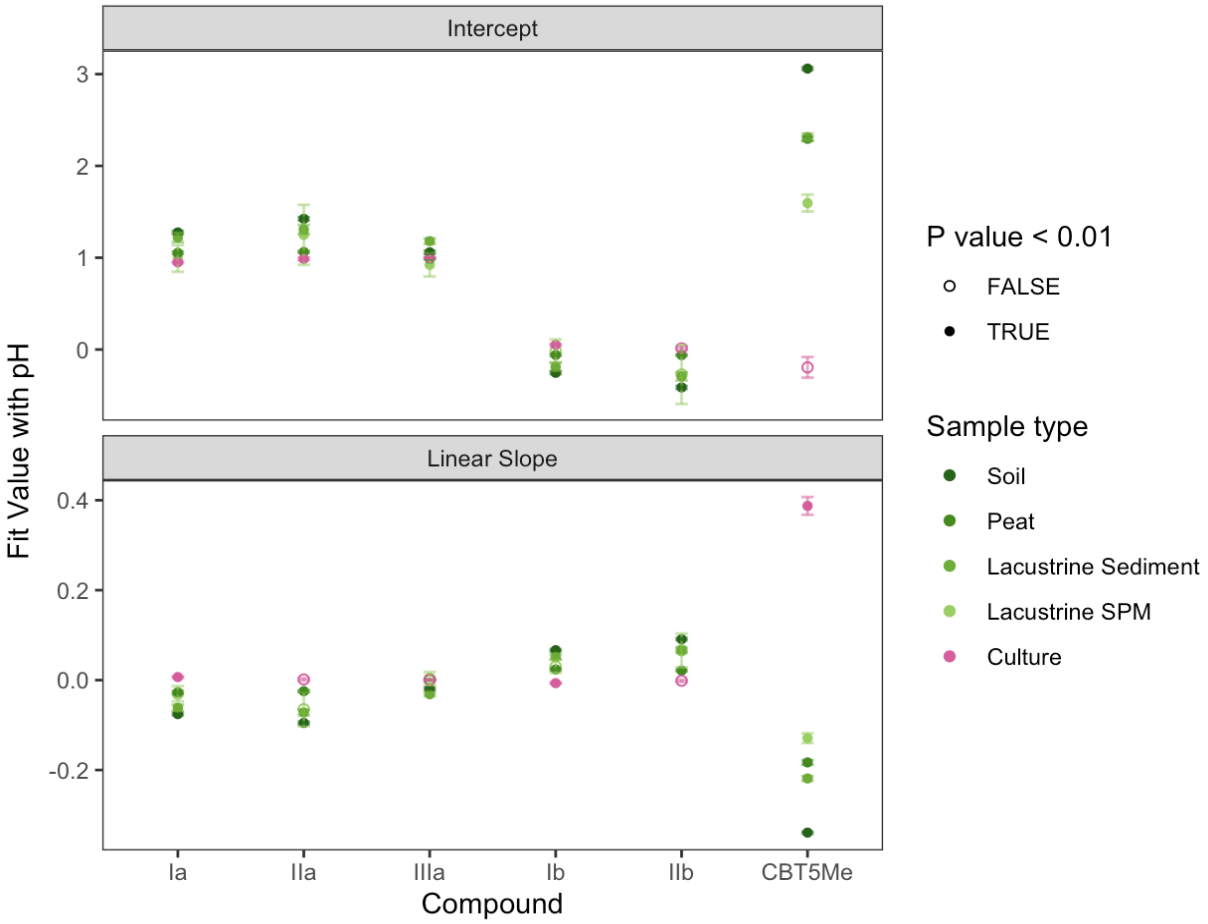

Fig. S7. Fitting coefficients for linear regressions between brGDGT Cyclization Set fractional abundances, CBT_{5Me}, and pH, as plotted in Figures S6 and 2F. Error bars represent one standard error. Coefficients with p values ≥ 0.01 are plotted as open circles.

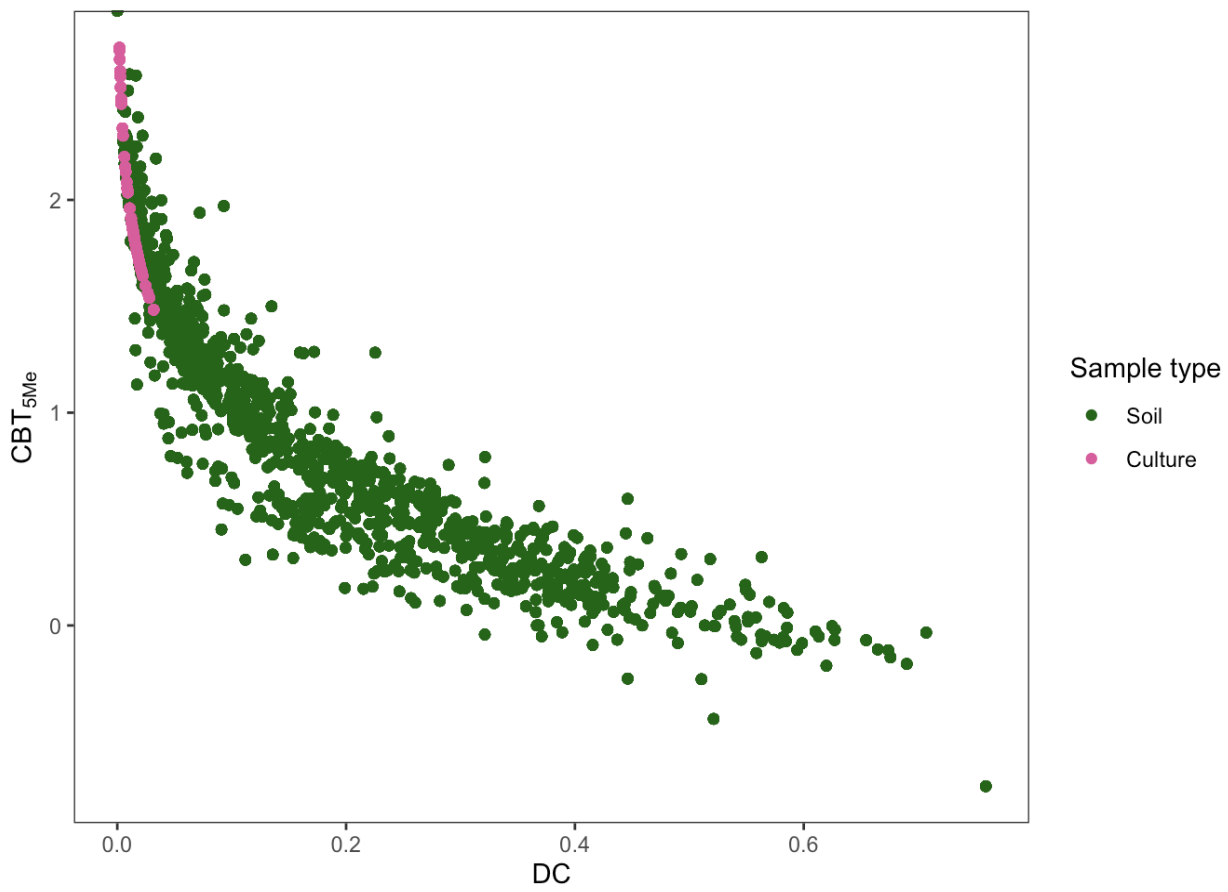

Fig. S8. Relationship between CBT_{5Me} and Degree of Cyclization (DC; Baxter et al., 2019), showing the high sensitivity of CBT_{5Me} when DC is low.

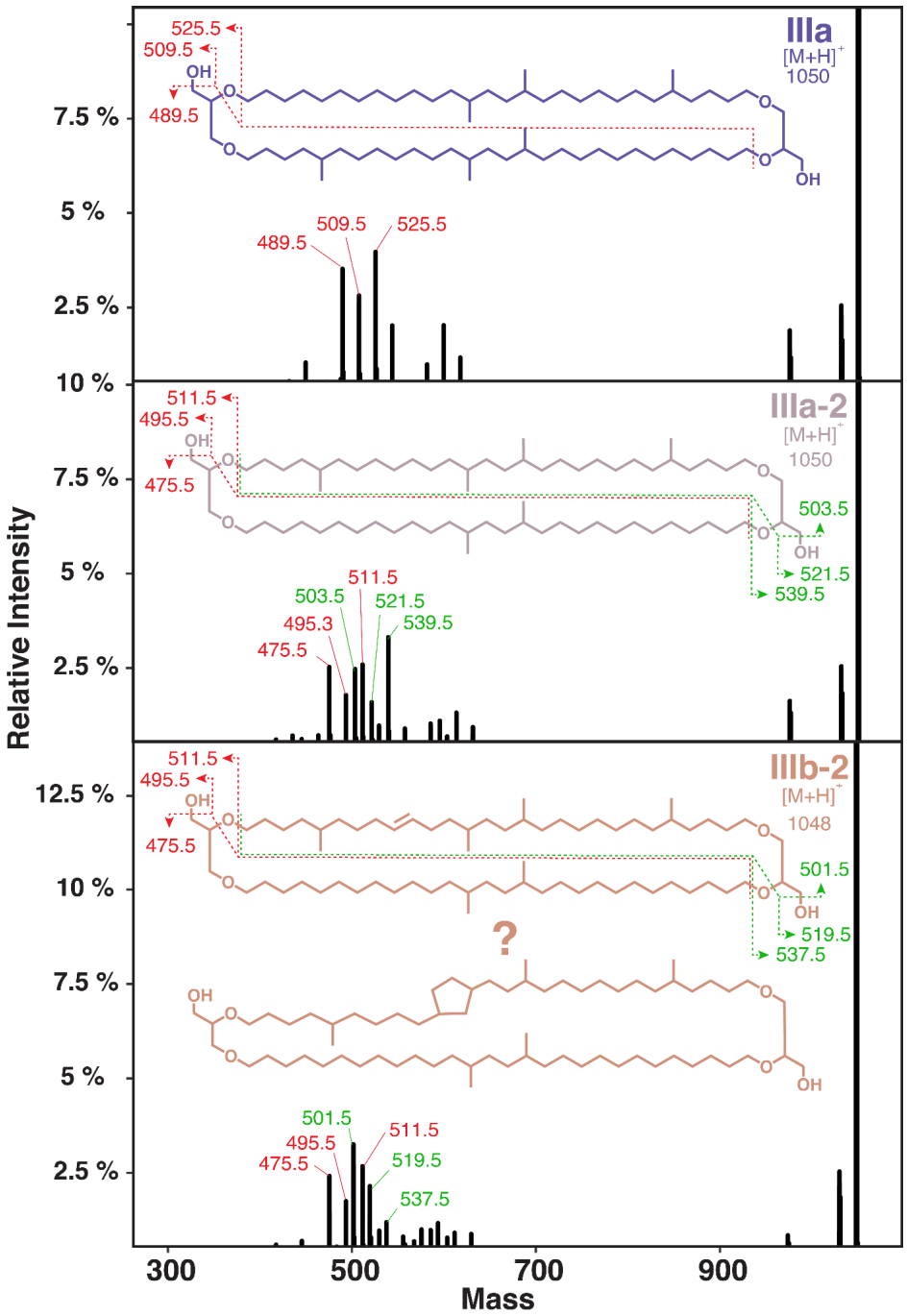

Fig. S9. MS/MS of hexa-methylated brGDGTs in *S. usitatus*. Characteristic fragments of each hexa-methylated brGDGT are highlighted in red and green (IIIa is symmetrical). The two alternative structures shown for IIIb-2 have identical mass fragments.

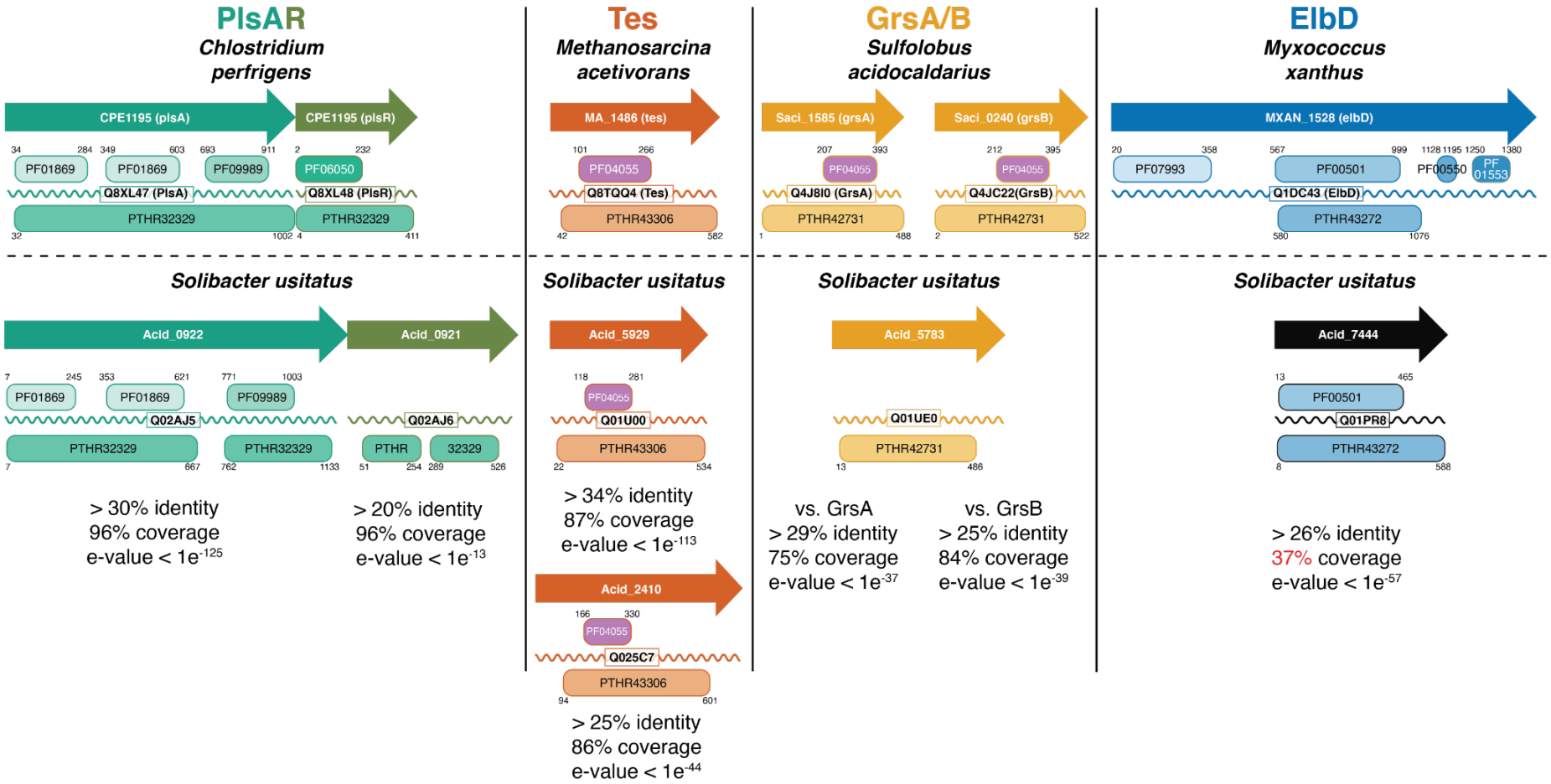

Fig. S10. Overview of *S. usitatus* homologs of proteins potentially involved in brGDGT biosynthesis. Genes are represented by arrows inscribed with gene loci. Proteins are represented by zigzag lines inscribed with UniProtIDs. Protein family and domain classifications (as predicted by Interpro scan, Hunter et al., 2014) are represented by rounded rectangles with PFAM (prefix "PF", Mistry et al., 2021) depicted above zigzag protein lines, and PANTHER (prefix "PTHR", Mi et al., 2013) depicted below zigzag protein lines. All representations are to scale with respect to amino acid sequence lengths. Proteins are color-coded for clarity except for the radical SAM domain (PF04055, in purple) which is part of both Tes and GrsA/B

proteins. Protein BLAST scores of *S. usitatus* homologs are provided below each protein (see Table S5 for details). PlsAR (ether lipid biosynthesis), Tes (tetraether synthesis) and GrsA/B (GDGT ring synthesis) from *Clostridium perfrigens*, *Methanosarcina acetivorans*, and *Sulfolobus acidocaldarius*, respectively, all have close homologs and domain structure in *S. usitatus*. ElbD (ether lipid biosynthesis) from *Myxococcus xanthus* and one of its BLAST results in *S. usitatus* is also included and shows how only the PF500501 portion of the protein (AMP-binding domain) matches proteins in *S. usitatus* (all with less than 40% coverage).

Supplementary Tables

Table S1. Culture growth rates (μ) for all experiments with *S. usitatus*. Growth rates were calculated for all replicates by fitting OD measurements to the logistic equation below using non-linear least squares regressions in R (t is time, fit parameters μ and K represent the growth rate and carrying capacity / max OD): $\boldsymbol{OD}\ (\boldsymbol{t}) = \frac{\boldsymbol{K}}{\boldsymbol{1+(K/OD_{t0}-1)\cdot e^{-\mu t}}}$. Growth rates of individual replicates are listed with the standard errors of the regression fit. Growth rate averages are listed with the standard deviation of the replicates.

Temperature (°C)	**pH**	**% O_2 (v/v)**	**Growth rates (day^{-1})**			
			Rep. 1	**Rep. 2**	**Rep. 3**	**Average**
15	5.0	21	0.25±0.02	0.36±0.06	0.28±0.03	0.30±0.06
15	5.5	21	0.28±0.02	0.31±0.03	0.28±0.02	0.29±0.02
15	6.0	21	0.26±0.03	0.17±0.01	0.26±0.03	0.23±0.05
20	5.0	21	0.37±0.02	0.35±0.01	0.42±0.02	0.38±0.03
20	5.5	21	0.58±0.06	0.52±0.05	0.46±0.01	0.52±0.06
20	6.0	21	0.50±0.03	0.58±0.05	0.57±0.04	0.55±0.05
20	6.5	21	0.58±0.04	0.51±0.03	0.53±0.04	0.54±0.04
25	5.0	21	0.43±0.01	0.53±0.02	0.52±0.05	0.49±0.05
25	5.5	21	0.73±0.03	0.83±0.03	0.79±0.02	0.78±0.05
25	6.0	21	1.04±0.11	1.01±0.10	1.00±0.10	1.02±0.02
25	6.5	21	1.07±0.09	1.00±0.08	0.70±0.07	0.92±0.20
30	5.0	21	0.73±0.07	1.16±0.21	0.70±0.06	0.86±0.26
30	5.5	21	1.48±0.29	1.41±0.24	1.47±0.30	1.45±0.03
30	6.0	21	1.12±0.12	1.13±0.13	1.16±0.14	1.14±0.02
30	6.5	21	0.82±0.05	0.94±0.08	1.00±0.09	0.92±0.09
25	5.5	5	0.50±0.00	0.66±0.00	0.54±0.00	0.57±0.09
25	5.5	1	0.36±0.00	0.30±0.00	0.34±0.00	0.33±0.03

Table S2. Overall membrane composition estimates for *S. usitatus* for all experimental conditions. Tetraether abundances were calculated relative to fatty acids and mono/di-ethers using the C24:0 fatty acid and C46 GTGT internal standards. Reported relative abundances are the statistical means and standard deviations of biological triplicates. The last column ('All') represents the statistical average and standard deviation across all experiments. See Dataset S1 for these data in spreadsheet format.

Experimental Conditions																		
T (°C)	**15**	**15**	**15**	**20**	**20**	**20**	**20**	**25**	**25**	**25**	**25**	**30**	**30**	**30**	**30**	**25**	**25**	**All**
pH	**5.0**	**5.5**	**6.0**	**5.0**	**5.5**	**6.0**	**6.5**	**5.0**	**5.5**	**6.0**	**6.5**	**5.0**	**5.5**	**6.0**	**6.5**	**5.5**	**5.5**	
% O2	**21**	**21**	**21**	**21**	**21**	**21**	**21**	**21**	**21**	**21**	**21**	**21**	**21**	**21**	**21**	**5**	**1**	
Major lipid classes' relative abundances in % (mean ± 1 standard deviation)																		
fatty acids	40.9 ±23.8	58.6 ±11.0	53.9 ±8.3	47.1 ±9.2	61.5 ±8.2	51.1 ±8.6	59.5 ±16.2	42.0 ±11.5	79.7 ±2.8	70.6 ±11.8	62.6 ±10.0	39.6 ±20.3	71.4 ±12.2	68.4 ±5.2	60.2 ±12.3	75.0 ±6.7	64.9 ±5.7	**59.2 ±12.1**
monoethers & diethers	12.1 ±4.0	16.8 ±2.2	20.9 ±5.4	19.0 ±0.9	12.8 ±3.3	14.9 ±1.0	14.6 ±6.1	34.3 ±1.5	10.2 ±2.9	12.8 ±4.4	20.5 ±2.0	38.5 ±14.9	15.6 ±7.4	15.4 ±2.1	18.3 ±8.8	4.7 ±0.3	3.4 ±0.7	**16.8 ±8.8**
tetraethers	47.0 ±23.7	24.7 ±8.8	25.2 ±3.4	33.8 ±9.7	25.7 ±5.2	34.0 ±8.3	25.9 ±10.7	23.7 ±10.1	10.1 ±0.1	16.6 ±7.4	16.9 ±10.4	22.0 ±5.6	13.0 ±4.9	16.1 ±3.1	21.5 ±4.8	20.3 ±6.7	31.6 ±5.0	**24.0 ±9.0**

Table S3. Liquid chromatography data including all branched GTGTs and branched GDGTs for *S. usitatus* for all experimental conditions. Relative abundances for each sample were calculated from TIC peak areas (n.q. = not quantified due to exceedingly low abundance or complete absence). Reported relative abundances are the statistical means and standard deviations of biological triplicates vs all listed compounds. Note that Fig. 3 visualizes abundances relative to the standard brGDGTs (Eq. 5) rather than the whole dataset listed here. The last column ('All') represents the statistical average and standard deviation across all experiments. See Fig. 1, Fig. 3 and Table S6 for chemical structures. See Dataset S1 for these data in spreadsheet format.

Experimental Conditions																		
T (°C)	**15**	**15**	**15**	**20**	**20**	**20**	**20**	**25**	**25**	**25**	**25**	**30**	**30**	**30**	**30**	**25**	**25**	**All**
pH	**5.0**	**5.5**	**6.0**	**5.0**	**5.5**	**6.0**	**6.5**	**5.0**	**5.5**	**6.0**	**6.5**	**5.0**	**5.5**	**6.0**	**6.5**	**5.5**	**5.5**	
% O2	**21**	**21**	**21**	**21**	**21**	**21**	**21**	**21**	**21**	**21**	**21**	**21**	**21**	**21**	**21**	**5**	**1**	
Branched GTGT relative abundances in % (mean ± 1 standard deviation)																		
brGTGT Ia	5.2 ±1.3	4.9 ±0.6	3.4 ±0.6	3.1 ±0.7	5.4 ±1.3	4.0 ±0.6	7.4 ±0.3	2.3 ±1.7	3.8 ±1.4	3.2 ±0.1	9.9 ±3.6	1.8 ±0.7	1.7 ±0.1	1.3 ±0.1	6.2 ±1.9	2.0 ±0.6	1.6 ±0.3	**4.0 ±2.3**
brGTGT IIa	0.31 ±0.16	0.18 ±0.05	0.12 ±0.04	1.1 ±0.4	0.53 ±0.32	0.21 ±0.03	0.09 ±0.02	0.99 ±1.53	1.7 ±0.1	0.35 ±0.02	0.11 ±0.04	0.14 ±0.13	0.28 ±0.01	0.18 ±0.02	0.06 ±0.01	0.69 ±0.11	0.44 ±0.16	**0.44 ±0.45**
brGTGT IIIa	0.20 ±0.08	0.14 ±0.04	0.11 ±0.03	0.49 ±0.14	0.41 ±0.10	0.17 ±0.01	0.11 ±0.01	0.53 ±0.56	1.1 ±0.5	0.28 ±0.01	0.11 ±0.04	0.32 ±0.04	0.33 ±0.01	0.22 ±0.03	0.19 ±0.01	3.8 ±0.9	0.91 ±0.22	**0.56 ±0.88**
Standard branched GDGT relative abundances in % (mean ± 1 standard deviation)																		
brGDGT Ia	55 ±2	51 ±3	42 ±2	80 ±3	76 ±2	74 ±0	72 ±0	92 ±3	90 ±2	93 ±0	89 ±4	95 ±1	96 ±0	96 ±0	93 ±2	82 ±1	89 ±1	**80 ±17**
brGDGT Ib	0.40 ±0.05	0.51 ±0.09	0.40 ±0.15	1.2 ±0.5	0.90 ±0.33	1.0 ±0.2	0.26 ±0.03	1.9 ±1.1	1.2 ±0.2	1.9 ±0.1	0.22 ±0.02	1.9 ±0.2	1.9 ±0.1	1.6 ±0.1	0.18 ±0.00	1.2 ±0.1	0.33 ±0.07	**1.0 ±0.7**
brGDGT Ic	n.q.	n.q.	n.q.	n.q.	n.q.	n.q.	n.q.	n.q.	n.q.	n.q.	n.q.	n.q.	n.q.	n.q.	n.q.	n.q.	n.q.	**n.q.**

brGDGT IIa	36 ±1	40 ±2	48 ±2	13 ±2	16 ±1	20 ±1	18 ±0	1.7 ±0.3	1.6 ±0.0	1.3 ±0.1	1.0 ±0.1	0.58 ±0.39	0.15 ±0.01	0.21 ±0.00	0.19 ±0.01	5.4 ±0.1	2.5 ±0.2	**12 ±16**
brGDGT IIb	0.25 ±0.04	0.44 ±0.16	0.43 ±0.24	n.q.	0.16 ±0.07	0.23 ±0.03	0.04 ±0.00	n.q.	n.q.	n.q.	n.q.	n.q.	n.q.	n.q.	n.q.	n.q.	n.q.	**0.09 ±0.16**
brGDGT IIc	n.q.	n.q.	n.q.	n.q.	n.q.	n.q.	n.q.	n.q.	n.q.	n.q.	n.q.	n.q.	n.q.	n.q.	n.q.	n.q.	n.q.	**n.q.**
brGDGT IIIa	2.9 ±0.2	3.3 ±0.4	5.2 ±0.6	0.99 ±1.24	0.30 ±0.02	0.46 ±0.04	2.4 ±0.1	0.04 ±0.01	0.05 ±0.03	0.05 ±0.01	0.05 ±0.01	0.07 ±0.05	0.03 ±0.00	0.03 ±0.00	0.06 ±0.00	0.03 ±0.00	0.01 ±0.00	**0.94 ±1.55**
brGDGT IIIb	n.q.	n.q.	n.q.	n.q.	n.q.	n.q.	n.q.	n.q.	n.q.	n.q.	n.q.	n.q.	n.q.	n.q.	n.q.	n.q.	n.q.	**n.q.**
brGDGT IIIc	n.q.	n.q.	n.q.	n.q.	n.q.	n.q.	n.q.	n.q.	n.q.	n.q.	n.q.	n.q.	n.q.	n.q.	n.q.	n.q.	n.q.	**n.q.**
Non-standard branched GDGT relative abundances in % (mean ± 1 standard deviation)																		
brGDGT IIIa-2	n.q.	n.q.	n.q.	0.05 ±0.01	0.03 ±0.01	0.02 ±0.00	n.q.	0.04 ±0.02	0.07 ±0.03	0.02 ±0.00	0.01 ±0.00	0.03 ±0.00	0.03 ±0.00	0.03 ±0.00	0.04 ±0.00	2.3 ±0.2	3.5 ±0.4	**0.36 ±0.97**
brGDGT IIIb-2	n.q.	n.q.	n.q.	0.14 ±0.02	0.08 ±0.04	0.02 ±0.00	0.01 ±0.00	0.14 ±0.15	0.26 ±0.10	0.02 ±0.00	0.01 ±0.00	0.05 ±0.01	0.04 ±0.00	0.04 ±0.00	0.07 ±0.01	2.7 ±0.2	1.7 ±0.2	**0.31 ±0.73**

Table S4. Gas chromatography data including fatty acids, mono-ethers and di-ethers for *S. usitatus* for all experimental conditions. Relative abundances for each sample were calculated from flame ionization detector (FID) peak areas (n.d. = not detected). Reported relative abundances are the statistical means and standard deviations of biological triplicates. Most unsaturated fatty acids (e.g., i15:1, i17:1, 18:1) were detected as multiple closely eluting isomers that reflect different positions of the double bond and were summed together for this data overview. The last column ('All') represents the statistical average and standard deviation across all experiments. See Table S6 for chemical structures and full names of key fatty acids and mono/diethers. See Dataset S1 for these data in spreadsheet format.

Experimental Conditions																		
T (°C)	**15**	**15**	**15**	**20**	**20**	**20**	**20**	**25**	**25**	**25**	**25**	**30**	**30**	**30**	**30**	**25**	**25**	**All**
pH	**5.0**	**5.5**	**6.0**	**5.0**	**5.5**	**6.0**	**6.5**	**5.0**	**5.5**	**6.0**	**6.5**	**5.0**	**5.5**	**6.0**	**6.5**	**5.5**	**5.5**	
% O2	**21**	**21**	**21**	**21**	**21**	**21**	**21**	**21**	**21**	**21**	**21**	**21**	**21**	**21**	**21**	**5**	**1**	
Fatty acid relative abundances in % (mean ± 1 standard deviation)																		
14:0	< 1	< 1	< 1	< 1	< 1	< 1	< 1	3.2 ±1.3	< 1	< 1	< 1	1.1 ±1.2	< 1	< 1	< 1	< 1	< 1	**< 1**
i15:1	1.6 ±1.8	1.2 ±1.3	< 1	< 1	3.7 ±1.7	1.6 ±0.8	1.7 ±2.2	< 1	5.4 ±2.8	4.6 ±3.0	1.6 ±0.4	< 1	4.0 ±3.6	2.2 ±1.5	< 1	9.8 ±0.3	3.4 ±0.1	**2.5 ±2.5**
i15:0	2.8 ±4.2	1.3 ±1.0	2.0 ±1.7	< 1	2.0 ±2.8	< 1	12.2 ±14.3	< 1	16.0 ±6.0	12.8 ±11.0	13.9 ±11.9	1.3 ±2.2	15.0 ±12.3	11.8 ±5.8	10.6 ±14.8	40.2 ±0.5	44.1 ±1.2	**11.0 ±13.2**
15:0	7.1 ±2.9	6.9 ±2.0	7.9 ±6.6	3.7 ±6.4	< 1	3.9 ±5.3	10.8 ±5.5	8.0 ±6.9	1.5 ±1.2	2.9 ±0.4	6.9 ±6.3	4.3 ±4.1	3.4 ±5.3	6.1 ±3.1	11.9 ±5.5	1.6 ±0.4	3.1 ±0.3	**5.3 ±3.2**
i16:0	< 1	< 1	< 1	< 1	< 1	< 1	< 1	< 1	< 1	< 1	< 1	< 1	< 1	< 1	< 1	< 1	< 1	**< 1**
16:1	2.3 ±2.6	4.3 ±1.8	3.7 ±1.5	1.8 ±0.6	5.0 ±1.1	4.8 ±1.0	2.3 ±0.9	< 1	4.9 ±0.6	6.8 ±0.6	3.3 ±1.1	1.3 ±1.6	4.8 ±2.2	5.3 ±1.0	1.7 ±0.8	6.9 ±0.4	9.4 ±0.6	**4.1 ±2.3**

16:0	< 1	1.3 ±0.3	< 1	1.5 ±0.2	1.7 ±0.4	1.6 ±0.2	3.0 ±0.8	< 1	2.0 ±0.4	1.1 ±0.2	3.2 ±0.2	< 1	1.3 ±0.3	1.5 ±0.1	2.6 ±0.5	< 1	3.3 ±0.3	**1.7 ±0.9**
i17:1	35.1 ±13.3	43.5 ±8.9	36.4 ±6.8	37.3 ±5.7	46.8 ±5.5	42.3 ±2.7	16.2 ±13.2	17.9 ±4.5	41.4 ±2.6	45.7 ±4.4	27.6 ±3.2	23.2 ±17.9	40.4 ±3.5	42.7 ±1.9	19.2 ±1.4	26.1 ±1.1	19.7 ±0.5	**33.0 ±10.8**
i17:0	2.7 ±0.7	3.2 ±0.7	2.0 ±0.3	3.0 ±0.9	3.1 ±0.4	3.0 ±0.4	18.5 ±4.9	2.9 ±1.3	2.9 ±0.5	2.9 ±0.7	10.5 ±9.1	3.2 ±1.8	3.7 ±0.7	3.7 ±0.4	17.4 ±2.0	1.6 ±0.1	3.1 ±0.3	**5.1 ±5.2**
17:1	6.3 ±7.1	4.8 ±3.3	8.3 ±4.9	5.0 ±1.6	6.3 ±0.9	6.8 ±0.7	4.3 ±2.9	6.4 ±5.6	3.4 ±1.1	1.1 ±0.2	< 1	3.0 ±4.9	3.7 ±4.5	< 1	2.8 ±1.1	3.7 ±0.4	3.7 ±0.9	**4.1 ±2.3**
17:0	5.2 ±0.7	3.9 ±2.7	4.2 ±2.7	6.1 ±1.7	6.6 ±1.7	5.0 ±1.5	3.7 ±1.6	3.5 ±2.7	4.8 ±1.9	1.0 ±0.2	2.2 ±2.3	< 1	< 1	1.1 ±0.2	2.2 ±1.3	1.7 ±0.5	2.1 ±0.2	**3.2 ±1.9**
18:1	5.1 ±4.8	2.6 ±0.5	2.5 ±0.2	4.2 ±0.6	2.3 ±0.2	2.9 ±0.7	2.0 ±0.8	2.4 ±1.0	2.0 ±0.4	1.9 ±0.6	1.5 ±0.2	2.7 ±1.2	1.6 ±0.2	2.1 ±0.4	2.1 ±0.5	< 1	1.5 ±0.1	**2.4 ±1.0**
18:0	3.4 ±1.0	2.7 ±0.5	2.5 ±0.7	4.4 ±0.4	2.9 ±0.3	3.5 ±0.9	2.8 ±0.9	5.2 ±1.5	2.8 ±1.1	1.8 ±0.6	2.7 ±1.1	4.1 ±0.1	1.9 ±0.6	2.5 ±0.5	3.6 ±1.3	< 1	< 1	**2.8 ±1.2**
19:1	< 1	< 1	< 1	1.4 ±0.5	< 1	< 1	< 1	1.6 ±0.4	< 1	< 1	< 1	1.6 ±0.7	< 1	< 1	< 1	< 1	< 1	**< 1**
20:0	< 1	< 1	< 1	1.1 ±0.1	< 1	< 1	< 1	1.8 ±0.6	< 1	< 1	< 1	1.9 ±0.5	< 1	< 1	< 1	< 1	< 1	**< 1**
iDA	n.d.	n.d.	n.d.	n.d.	n.d.	n.d.	n.d.	n.d.	n.d.	n.d.	n.d.	n.d.	n.d.	n.d.	n.d.	n.d.	n.d.	**n.d.**
Mono/diether relative abundances in % (mean ± 1 standard deviation)																		
1-i15:0 MAGE	6.4 ±2.5	5.9 ±2.3	11.4 ±5.6	7.9 ±2.9	4.3 ±1.4	6.0 ±0.6	12.3 ±6.1	23.1 ±14.6	1.7 ±0.2	5.5 ±3.5	11.2 ±3.8	21.5 ±14.9	5.2 ±2.7	6.4 ±1.2	11.8 ±4.1	1.8 ±0.1	3.3 ±1.0	**8.6 ±6.1**
2-i15:0 MAGE	2.7 ±1.4	1.4 ±0.3	1.2 ±0.4	2.3 ±1.2	1.5 ±0.2	< 1	< 1	1.9 ±0.5	< 1	< 1	< 1	1.5 ±0.7	< 1	< 1	< 1	< 1	< 1	**1.1 ±0.7**
1,2-i15:0 DAGE	16.6 ±7.3	15.3 ±4.8	15.5 ±4.5	18.9 ±1.0	11.7 ±3.9	15.8 ±3.8	7.4 ±3.7	20.7 ±8.9	9.1 ±2.8	9.7 ±3.4	13.1 ±2.5	27.3 ±10.1	12.6 ±6.9	11.6 ±1.9	11.1 ±9.8	3.7 ±0.7	1.2 ±0.2	**13.0 ±6.2**

Table S5. Protein BLAST results from the *S. usitatus* Ellin6076 proteome (https://www.uniprot.org/proteomes/UP000000671, retrieved Feb. 27 2022) for proteins potentially involved in brGDGT biosynthesis (e-value < $1e^{-10}$). See Figure S10 for domain visualizations.

Protein	Query				BLASTP results from *S. usitatus* Ellin6076					
	Organism	**Gene Locus**	**UniProt ID**	**AAs**	**Gene Locus**	**UniProt ID**	**AAs**	**Coverage**	**Identity**	**e-value**
PlsA	*Clostridium perfringens*	CPE1195	Q8XL47	1004	Acid_0922	Q02AJ5	1188	96%	30.2%	1.48e-126
PlsR	*Clostridium perfringens*	CPE1194	Q8XL48	420	Acid_0921	Q02AJ6	589	96%	20.9%	2.33e-14
Tes	*Methanosarcina acetivorans*	MA_1486	Q8TQQ4	584	Acid_5929	Q01U00	545	87%	34.7%	3.02e-114
					Acid_2410	Q025C7	714	86%	26.0%	4.04e-45
GrsA	*Sulfolobus acidocaldarius*	Saci_1585	Q4J8I0	489	Acid_5783	Q01UE0	597	75%	29.3%	3.90e-38
GrsB	*Sulfolobus acidocaldarius*	Saci_0240	Q4JC22	528	Acid_5783	Q01UE0	597	84%	25.2%	1.29e-40
ElbD	*Myxococcus xanthus*	MXAN_1528	Q1DC43	1470	Acid_7444	Q01PR8	597	37%	26.4%	1.29e+57
					Acid_0997	Q02AC7	468	31%	30.9%	4.88e-51
					Acid_5700	Q01UM3	554	30%	30.0%	1.80e-45
					Acid_3608	Q020R4	540	36%	27.7%	6.05e-44
					Acid_1327	Q029G6	496	32%	27.7%	1.55e-04

Table S6. Chemical structures of compounds discussed in the manuscript that are not already included in other figures (like the brGDGTs in Fig. 1 and Fig. 3).

FAs (fatty acids)
i15:0 FA (*iso* C15:0 fatty acid) 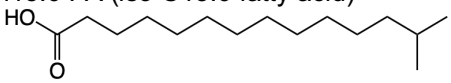
iDA (*iso* diabolic acid / 13,16-dimethyl-octacosanedioic acid) 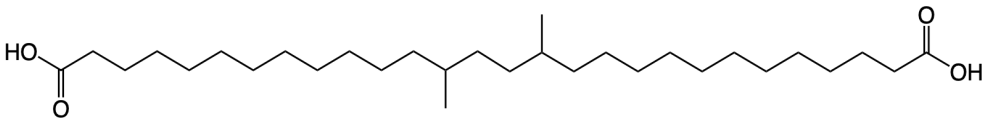
MAGEs (monoalkyl/monoalkanoic glycerol monoethers)
i15:0 MAGE (1-*iso* C15:0 monoalkyl glycerol monoether) aka 1-*iso* C15 MGE 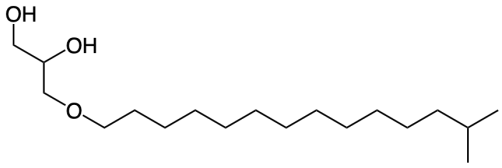
i15:0 MAGE (2-*iso* C15:0 monoalkyl glycerol monoether) aka 2-*iso* C15 MGE 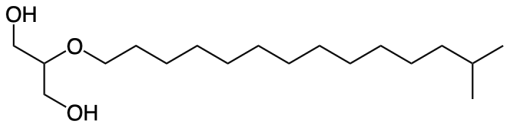
iDA MAGE (*iso*-diabolic acid monoalkanoic glycerol monoether) aka *iso*-diabolic acid MGE 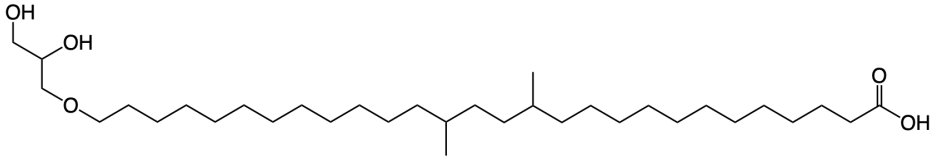
DAGEs (dialkyl/dialkanoic glycerol diethers)
1,2-i15:0 DAGE (1,2-*iso* C15:0 dialkyl glycerol diether) aka 1,2-*iso* C15 DGE 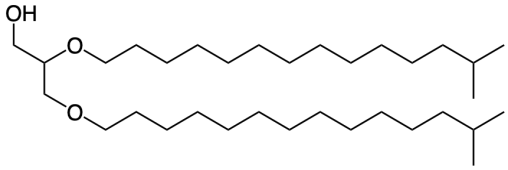

1,2-iDA DAGE (1,2-*iso* diabolic acid dialkanoic glycerol diether)

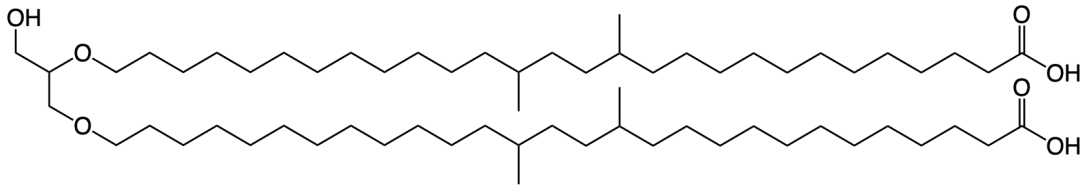

GDGTs (glycerol dialkyl glycerol tetraethers)

See Fig. 1 for all standard branched GDGT structures (Ia, b, c; IIa, b, c; IIIa, b, c).

See Fig. 3 for non-standard branched GDGT structures (IIIa-2, IIIb-2).

GTGTs (glycerol trialkyl glycerol tetraethers)

brGTGT Ia

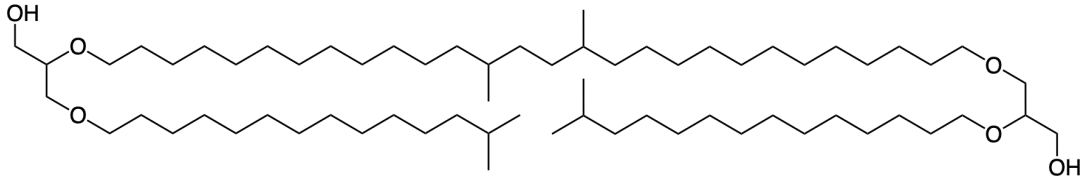

brGTGT IIa

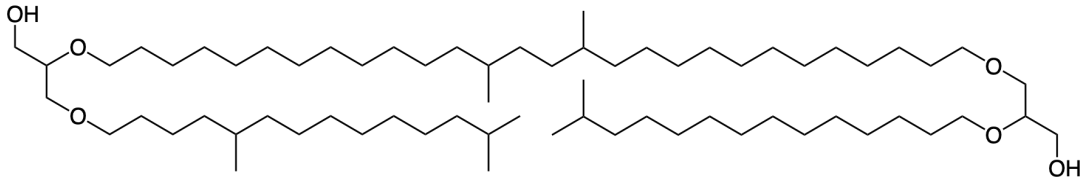

brGTGT IIIa

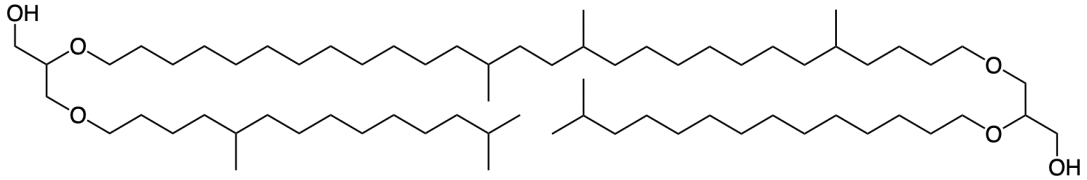

SI References

Baxter, A. J., Hopmans, E. C., Russell, J. M., & Sinninghe Damsté, J. S. (2019). Bacterial GMGTs in East African lake sediments: Their potential as palaeotemperature indicators. *Geochimica et Cosmochimica Acta*, *259*, 155–169. https://doi.org/10.1016/j.gca.2019.05.039

Hunter, S., Apweiler, R., Attwood, T. K., Bairoch, A., Bateman, A., Binns, D., Bork, P., Das, U., Daugherty, L., Duquenne, L., Finn, R. D., Gough, J., Haft, D., Hulo, N., Kahn, D., Kelly, E., Laugraud, A., Letunic, I., Lonsdale, D., … Yeats, C. (2009). InterPro: The integrative protein signature database. *Nucleic Acids Research*, *37*(Database), D211–D215. https://doi.org/10.1093/nar/gkn785

Mi, H., Muruganujan, A., & Thomas, P. D. (2012). PANTHER in 2013: Modeling the evolution of gene function, and other gene attributes, in the context of phylogenetic trees. *Nucleic Acids Research*, *41*(D1), D377–D386. https://doi.org/10.1093/nar/gks1118

Mistry, J., Chuguransky, S., Williams, L., Qureshi, M., Salazar, G. A., Sonnhammer, E. L. L., Tosatto, S. C. E., Paladin, L., Raj, S., Richardson, L. J., Finn, R. D., & Bateman, A. (2021). Pfam: The protein families database in 2021. *Nucleic Acids Research*, *49*(D1), D412–D419. https://doi.org/10.1093/nar/gkaa913

Raberg J. H., Miller G. H., Geirsdóttir Á. and Sepúlveda J. (2022a) [in press], Near-universal trends in brGDGT lipid distributions in nature.

Raberg, J. H., Harning, D. J., Crump, S. E., de Wet, G., Blumm, A., Kopf, S., Geirsdóttir, Á., Miller, G. H., & Sepúlveda, J. (2021). Revised fractional abundances and warm-season temperatures substantially improve brGDGT calibrations in lake sediments. *Biogeosciences*, *18*(12), 3579–3603. https://doi.org/10.5194/bg-18-3579-2021